

1 **Fast Transport of RNA Granules by Direct Interactions with KIF5A/KLC1 Motors Prevents Axon**
2 **Degeneration**

3
4 **Yusuke Fukuda^{1,2}, Maria F. Pazyra-Murphy^{1,2}, Ozge E. Tasdemir-Yilmaz^{1,2}, Yihang Li^{1,2}, Lillian Rose^{1,2}, Zoe**
5 **C. Yeoh², Nicholas E. Vangos², Ezekiel A. Geffken², Hyuk-Soo Seo^{2,3}, Guillaume Adelmant^{2,4}, Gregory H.**
6 **Bird^{2,5,6}, Loren D. Walensky^{2,5,6}, Jarrod A. Marto^{2,4}, Sirano Dhe-Paganon^{2,3}, and Rosalind A. Segal^{1,2,7,*}**

7
8 ¹Department of Neurobiology, Harvard Medical School, Boston, MA 02115, USA

9 ²Department of Cancer Biology, Dana-Farber Cancer Institute, Boston, MA 02115, USA

10 ³Department of Biological Chemistry & Molecular Pharmacology, Harvard Medical School, Boston, MA
11 02115, USA

12 ⁴Blais Proteomics Center, Dana-Farber Cancer Institute, Boston, MA 02115, USA

13 ⁵Linde Program in Cancer Chemical Biology, Dana-Farber Cancer Institute, Boston, MA 02115, USA

14 ⁶Department of Pediatric Oncology, Dana-Farber Cancer Institute, Boston, MA 02115, USA

15 ⁷Lead Contact

16 *Correspondence: rosalind_segal@dfci.harvard.edu (R.A.S.)

17

18

19

20 **Abstract**

21 Complex neural circuitry requires stable connections formed by lengthy axons. To maintain these

22 functional circuits, fast transport delivers RNAs to distal axons where they undergo local translation.

23 However, the mechanism that enables long distance transport of non-membrane enclosed organelles

24 such as RNA granules is not known. Here we demonstrate that a complex containing RNA and the RNA-

25 binding protein (RBP) SFPQ interacts directly with a tetrameric kinesin containing the adaptor KLC1 and

26 the motor KIF5A. We show that binding of SFPQ to KIF5A/KLC1 motor complex is required for axon survival

27 and is impacted by KIF5A mutations that cause Charcot-Marie-Tooth (CMT) Disease. Moreover,

28 therapeutic approaches that bypass the need for local translation of SFPQ-bound proteins prevent axon

29 degeneration in CMT models. Collectively, these observations show that non-membrane enclosed

30 organelles can move autonomously and that replacing axonally translated proteins provides a therapeutic

31 approach to axonal degenerative disorders.

32 Introduction

33 Sensory and motor neurons transmit signals through axons than can exceed a meter in length.
34 Therefore, many axonal functions, including axonal survival pathways, depend on proteins that are locally
35 translated and replenished in axon terminals. Localized protein synthesis is enabled by the initial assembly
36 of mRNAs and RNA-binding proteins (RBPs) into ribonucleoprotein (RNP) granules which occurs within the
37 cell soma, transport of these RNA granules to axon endings, and subsequent release of RNA for local
38 protein synthesis (Das, Singer, & Yoon, 2019). Human mutations that disrupt RNA granule formation,
39 interfere with cytoskeletal structures, or alter activity of intracellular motors and thus interfere with
40 granule transport are a major cause of neurologic diseases including amyotrophic lateral sclerosis (ALS),
41 hereditary spastic paraplegia (HSP) and Charcot-Marie-Tooth (CMT) disease. Degeneration of axons
42 occurs early in such neurodegenerative disorders and precedes cell death of the affected neurons.

43 While transport of RNA granules to axons is an important step in the homeostasis of RNA and
44 proteins in axons, the mechanism by which these non-membrane enclosed organelles are transported by
45 microtubule-dependent motors is not yet understood. A recent study revealed one mechanism for long-
46 range axonal transport in which *actin*-containing RNA granules “hitchhike” on lysosomes (Liao et al., 2019).
47 However, it is not known if this represents a uniform mechanism for transport of diverse RNA-granules,
48 or whether some types of RNA granules can be transported by motors independently of membrane
49 containing structures.

50 Splicing factor proline/glutamine-rich (SFPQ) is a ubiquitous RBP that has critical functions in
51 axons of both sensory and motor neurons (Cosker, Fenstermacher, Pazyra-Murphy, Elliott, & Segal, 2016;
52 Pease-Raissi et al., 2017; Thomas-Jinu et al., 2017). In sensory neurons, SFPQ assembles neurotrophin-
53 regulated transcripts, such as *bclw* and *Imnb2*, to form RNA granules, and is required for axonal
54 localization of these mRNAs and their subsequent translation (Cosker et al., 2016; Pease-Raissi et al.,
55 2017) . Similar to many other RBPs, SFPQ contains an intrinsically disordered region (**Introduction-figure**

56 **supplement 1)** and has been demonstrated to be a component of large RNA transport granules in neurons
57 (Kanai, Dohmae, & Hirokawa, 2004). Thus, loss of SFPQ leads to depletion of axonal mRNAs and results in
58 axon degeneration in dorsal root ganglion (DRG) sensory neurons (Cosker et al., 2016). Similarly, SFPQ is
59 critical for the development and maintenance of motor neuron axons (Thomas-Jinu et al., 2017). Missense
60 mutations in the coiled coil region of SFPQ have been identified that cause familial ALS and impair the
61 localization of SFPQ within distal axon segments (Thomas-Jinu et al., 2017). However, we do not yet
62 understand the mechanisms by which this RBP organizes mRNA transport granules that can then move
63 rapidly to distal axons where the mRNA cargos are released and translated.

64 Three distinct, but closely related genes, *KIF5A*, *KIF5B* and *KIF5C*, encode the conventional kinesin-
65 1 family of motor heavy chains, which are required for anterograde axonal transport of diverse organelles.
66 Mutations in *KIF5A* cause axonal degenerative disorders including CMT Type 2D (CMT2D), HSP and ALS
67 (Millecamps & Julien, 2013; Sleight, Rossor, Fellows, Tosolini, & Schiavo, 2019). It has been proposed that
68 *KIF5A* mutations may cause neurologic diseases by affecting transport efficiency overall. However,
69 mutations in *KIF5B* or *KIF5C* do not cause similar neurologic disorders, suggesting that mutations in *KIF5A*
70 may instead initiate disease due to impaired transport of *KIF5A*-specific cargo(s). Here, we show that the
71 degeneration of axons in *KIF5A* or SFPQ-mutant neurons reflects failure to transport a specific non-
72 membrane enclosed organelle rather than a general loss of transport. We identify this cargo as SFPQ-RNA
73 granules and show that a stable small peptide that mimics the function of a locally translated protein can
74 rescue degeneration caused by defective axonal transport.

75 **Results**

76 **SFPQ granule, a non-membrane enclosed organelle, undergoes fast axonal transport.**

77

78 The RBP SFPQ is found in both cell bodies and axons of sensory neurons. However, the
79 mechanisms by which SFPQ and its critical RNA cargos are transported between these two locations is
80 not known. We utilized live cell imaging of DRG sensory neurons expressing Halo-tagged SFPQ to directly
81 visualize transport dynamics (**Video 1**). Fluorescent signal was enriched in the nucleus and was also
82 evident as discrete granules in the soma and axons, a pattern similar to the distribution of endogenous
83 SFPQ (Cosker et al., 2016). Consistent with the presence of intrinsically disordered regions within the
84 SFPQ coding sequence, Halo-tagged SFPQ granules exhibited liquid like properties during time-lapse
85 imaging (Gopal, Nirschl, Klinman, & Holzbaur, 2017), as the size and shape of SFPQ granules remained
86 constant at approximately 1 μm in diameter during the stationary phase, but the granules expanded and
87 elongated as they move (**Figure 1A and 1B**). The majority of the Halo-tagged SFPQ granules in axons
88 were motile, either moving by retrograde transport (~48%), or anterograde transport (~28%), with the
89 remainder in stationary phase (~25%) (**Figure 1C and Figure 1-figure supplement 1A**). SFPQ granules
90 exhibit an average anterograde velocity of $0.89 \pm 0.08 \mu\text{m}/\text{sec}$ and average anterograde cumulative
91 displacement of $21.02 \pm 2.49 \mu\text{m}$, with an average retrograde velocity of $0.80 \pm 0.04 \mu\text{m}/\text{sec}$ retrograde
92 and average retrograde cumulative displacement of $32.02 \pm 2.45 \mu\text{m}$ (**Figure 1D, Figure 1-figure**
93 **supplement 1B-E**). Together, the velocity and the characteristics of movement indicate that the SFPQ-
94 granules are non-membrane enclosed organelles that move in both directions by microtubule-
95 dependent fast axonal transport, using a kinesin motor for anterograde and the more highly processive
96 dynein motor for retrograde movements.

97

98

99

100 **SFPQ preferentially binds to KIF5A/KLC1 motor complex.**

101 The anterograde kinesins involved in axon transport are formed by two dimers of kinesin heavy
102 chain (KHC or KIF5) and two dimers of kinesin light chain (KLC) (**Figure 2A**). The KIF5 family is encoded by
103 three distinct genes, *KIF5A*, *KIF5B* and *KIF5C*, and the genome also contains several light chains, KLC1-4.
104 To identify motors that associate with SFPQ and might enable transport of these RNA granules, we took
105 an unbiased approach in which we immunoprecipitated endogenous SFPQ from DRG neurons and used
106 mass spectrometry to analyze the co-precipitated components. We detected known interactors, including
107 the *Drosophila* behavior/human splicing (DBHS) protein family members NONO and PSPC1 in the
108 precipitated proteins (**Supplementary File 1**). We then analyzed the relative abundance of KIF5A, KIF5B
109 and KIF5C (**Figure 2B**) and KLC1, KLC2 (**Figure 2C**) in the SFPQ immunoprecipitates using a targeted mass
110 spectrometry approach. We found that KIF5A and KLC1 were each highly enriched over the other proteins
111 (KIF5B or KIF5C and KLC2, respectively) as measured across three independent experiments (**Figure 2B,**
112 **2C and Figure 2-figure supplement 1A**). In contrast, when we purified endogenous KLC1 from DRG
113 neurons and analyzed the composition of the resulting immunoprecipitate by mass spectrometry, we
114 observed that all three KIF5 proteins were present at approximately the same abundance in KLC1
115 immunoprecipitate (**Figure 2-figure supplement 1A and 1B**). Similarly, validated antibodies specific to
116 each of the three KIF5s (**Figure 2-figure supplement 1C and 1D**) corroborate that SFPQ preferentially co-
117 immunoprecipitates with KIF5A, rather than the closely related KIF5B or KIF5C (**Figure 2D and 2E**), and
118 with KLC1 rather than KLC2 (**Figure 2F**). Together these results suggest the possibility that KIF5A/KLC1
119 tetramers may be the distinctive motors responsible for rapid anterograde transport of SFPQ-RNA
120 granules.

121 A previous study of kinesin-1 motors demonstrates that overexpressed KIF5A, B and C can all
122 traffic to axons, but KIF5A is excluded from dendrites (Lipka, Kapitein, Jaworski, & Hoogenraad, 2016).
123 DRG sensory neurons are pseudo-unipolar in morphology and so have no dendrites, but instead consist

124 of a cell body with a T-shaped axon. To determine whether the intracellular distribution of kinesins is
125 consistent with the hypothesis that KIF5A/KLC1 is the motor that transports SFPQ-RNA granules, we
126 cultured DRG sensory neurons in compartmented cultures and collected protein lysates distinctly from
127 cell body (CB) and distal axon (DA) compartments. While KIF5B preferentially localizes in the CB
128 compartment, KIF5A and KIF5C localize to both CB and DA compartments, as do KLC1 and KLC2 (**Figure**
129 **2G**). Immunostaining of KIF5s in DRG neurons cultured in microfluidic chambers as well as DRGs and sciatic
130 nerves *in vivo* displayed a similar localization pattern, with KIF5B largely excluded from axons (**Figure 2H**
131 **and Figure 2-figure supplement 2**). Together these data demonstrate that KIF5A and KLC1 are
132 appropriately localized to mediate transport of SFPQ-RNA granules from cell bodies to distal axons, and
133 thus KIF5A/KLC1 may represent a specialized motor for these non-membrane enclosed organelles.

134

135 **RNase prevents SFPQ-RNA binding to KIF5A/KLC1.**

136 As RNA is a critical component of the large SFPQ-containing granules that move rapidly within the
137 axons, we asked whether SFPQ that binds to KIF5A/KLC1 is also associated with RNA cargos. We expressed
138 HA-SFPQ, FLAG-KIF5A and KLC1-Myc in HEK293T cells, and treated the cell lysates with RNase, or vehicle
139 control, and then immunoprecipitated for HA-SFPQ. Strikingly we find that RNase treatment impeded the
140 interaction between SFPQ and KIF5A-KLC1 (**Figure 3A-C**), demonstrating that SFPQ only binds KIF5A/KLC1
141 when it is associated with RNA. These findings suggest that KIF5A/KLC1 bind and transport SFPQ when it
142 is part of a large RNP transport granule.

143 Based on the above findings, we hypothesize that KIF5A/KLC1 distinctively mediates fast transport
144 of critical SFPQ-RNA granules from the cell soma to the axons. To identify the structural basis for this
145 specificity, we first asked whether the highly divergent C-terminal tail regions of KLC1 and KIF5A are
146 required for SFPQ binding. When we overexpressed either Myc-tagged WT KLC1 or its C-terminal mutant
147 (Δ Tail) in HEK 293T cells, and assessed binding to SFPQ by co-precipitation studies, we find that the binding

148 is reduced by approximately 50% in the absence of the C-terminal region of KLC1 (**Figure 3D-F**). Similarly,
149 truncation of the highly variable tail region of KIF5A nearly abolished its interaction with SFPQ (**Figure 3G-**
150 **I**) although this did not prevent binding of KIF5A to KLC1 (**Figure 3-figure supplement 1**). Together these
151 data demonstrate that SFPQ binding to KIF5A/KLC1 is enabled by the highly divergent C-terminal regions
152 of both KLC1 and KIF5A.

153

154 **SFPQ directly binds to KLC1 through a Y-acidic motif within its coiled coil domain.**

155 Evidence that SFPQ binding to KIF5A/KLC1 requires concurrent binding to RNA, suggests that this
156 RBP may directly link RNA transport granules to kinesin motors, enabling these RNA granules to move
157 autonomously without a membranous platform. To develop novel tools for testing this possibility, we
158 sought to identify specific mutations in SFPQ that impair binding to kinesin. SFPQ contains a Y-acidic motif
159 that is evolutionary conserved and closely matches the Y-acidic sequence of JIP1 that connects
160 membranous organelles to KLC1 (Nguyen et al., 2018; Pernigo et al., 2018) (**Figure 4A and Figure 4-figure**
161 **supplement 1**). When we mutated the critical tyrosine residue within the motif to alanine (Y527A) the
162 binding between SFPQ and KIF5A/KLC1 was dramatically reduced, demonstrating that this Y-acidic motif
163 is required for binding to KIF5A/KLC1 motor complex (**Figure 4B and 4C**). To assess whether SFPQ binds
164 directly to KLC1 without requiring a membranous organelle or an adaptor component, we purified human
165 KLC1 and used isothermal titration calorimetry (ITC) to test direct binding by a long SFPQ peptide that
166 spans the Y-acidic motif. The SFPQ peptide binds directly to KLC1 with a K_d of $3.8 \pm 2.3 \mu\text{M}$ and a binding
167 stoichiometry of 1 (**Figure 4D and Table 1**). Consistent with data from co-immunoprecipitation studies
168 above, Y527A mutation prevents the SFPQ peptide from binding directly to KLC1 in ITC assays (**Figure 4D**).
169 Thermodynamic parameters of ITC measurements are summarized in Table 1. Together these data
170 demonstrate that SFPQ directly binds to KLC1 in a process that relies on the Y-acidic motif and is abrogated
171 by the Y527A mutation. These studies suggest that SFPQ RNA-transport granules might directly associate

172 with microtubule-dependent motors rather than requiring a membrane platform for intracellular
173 transport.

174

175 **Direct binding of SFPQ to KIF5A/KLC1 is required for its transport in axons.**

176 The Y527A mutant of SFPQ provides a tool that can be used to ask whether the direct interaction
177 between SFPQ and kinesin motors is responsible for autonomous transport of SFPQ-RNA granules along
178 microtubules. Such a transport mechanism would contrast with previous models for transport of non-
179 membrane enclosed granules, as RNA granules that contain β -actin *mRNA* “hitchhike” on membrane
180 platforms, and do not move autonomously (Liao et al., 2019). To determine whether the direct binding of
181 SFPQ-RNA granules to kinesin mediates fast axonal transport, we expressed Halo-tagged WT or Y527A
182 SFPQ within DRG neurons grown in microfluidic chambers. In neurons expressing the Y527A mutant
183 **(Video 2)**, the number of SFPQ particles localized to distal axons was reduced by ~50%, suggesting that
184 direct binding of SFPQ to KIF5A/KLC1 is required for the redistribution of SFPQ-granules from the cell
185 bodies to distal axons **(Figure 5A and 5B)**. Moreover, among the SFPQ granules that reached the axons,
186 the Y527A mutant SFPQ exhibited a ~50% reduction in the percentage of time spent in anterograde axonal
187 transport compared to WT **(Figure 5C)**. Since SFPQ forms a dimer, residual movement of Y527A may
188 reflect binding of KIF5A/KLC1 motors to dimeric SFPQ containing both endogenous WT SFPQ and the
189 fluorescent mutant isoform (Hewage, Caria, & Lee, 2019). Together these data demonstrate that defects
190 in the direct binding of Y527A to KIF5A/KLC1 motor complex interrupts anterograde transport of RNA
191 granules in axons of DRG sensory neurons, suggesting that these RNA granules move autonomously and
192 do not require a membrane platform.

193 It is striking that the Y-acidic motifs in JIP1 and other proteins that link kinesins to membranous
194 organelles are usually located within highly accessible regions such as the carboxy terminus, while the Y-
195 acidic motif in SFPQ is instead located within the highly structured coiled-coil domain. These structural

196 differences suggest that SFPQ-RNA granules may interact with kinesin in a different manner than do
197 membranous organelles. Previous studies identified sequences within KLC1 that are not present in KLC2
198 and that specify binding to JIP1. One key residue in KLC1 is N343 within the TPR4 region of KLC1; mutation
199 of this residue to a serine, as observed in KLC2, abrogates interaction between JIP1 and KLC1 (Zhu et al.,
200 2012) (**Figure 5-figure supplement 1A**). To determine whether N343 on KLC1 also mediates binding to
201 SFPQ, we expressed myc-tagged WT or N343S KLC1 together with HA-tagged SFPQ in HEK 293T cells. We
202 find that KLC1-N343S did not alter binding to SFPQ, in clear contrast to JIP1 (**Figure 5-figure supplement**
203 **1B**), suggesting that the way in which SFPQ-RNA granules bind to kinesin motors for transport differs from
204 that observed with JIP1.

205

206 **Defect in KIF5A-driven transport of SFPQ leads to axon degeneration in DRG sensory neurons.**

207 To determine the physiologic consequences of impeding SFPQ transport by KIF5A/KLC1, we
208 leveraged the SFPQ Y527A mutant (**Figure 6A and 5**). As shown previously, knockdown of SFPQ results in
209 axon degeneration . We then assessed the ability of constructs encoding either the WT SFPQ or SFPQ-
210 Y527A to reverse the degeneration caused by knockdown, using constructs resistant to shRNA knockdown
211 (**Figure 6B and Figure 6-figure supplement 1**). Strikingly, expression of the WT version rescued axon
212 degeneration caused by knockdown of SFPQ, whereas expression of SFPQ Y527A was unable to do so, and
213 instead led to the same degree of axon degeneration observed following knockdown of SFPQ (**Figure 6C**
214 **and 6D**). Taken together these data indicate that autonomous transport of SFPQ-RNA granules is required
215 for axon survival and demonstrate that defects in kinesin-driven transport of SFPQ causes degeneration
216 of sensory axons.

217 Our data indicate that KIF5A/KLC1 functions as the motor transporting SFPQ-RNA granules within
218 DRG sensory neurons, and that this distinct transport process is required for axon survival. Thus, CMT2D
219 mutations of KIF5A may cause defects in this specialized transport pathway and so compromise axonal

220 health. Mutations causing HSP and CMT2D are located primarily within the motor domain of KIF5A; each
221 distinct mutation can give rise to HSP or CMT2D or a combination of both syndromes. Two independent
222 studies have reported a R280H mutation that results in a pure classical form of CMT2D (**Figure 6A**) (Liu et
223 al., 2014; Nam, Yoo, Choi, Choi, & Chung, 2018). Both structural and biochemical characterization
224 indicates that disease mutations altering this residue reduce the microtubule binding affinity, and
225 therefore decrease transport (Dutta, Diehl, Onuchic, & Jana, 2018; Ebbing et al., 2008; Fuger et al., 2012;
226 Jennings et al., 2017). Interestingly, despite the mutation residing within the motor domain, R280H
227 mutation also reduced binding to SFPQ approximately 25% compared to WT KIF5A (**Figure 6-figure**
228 **supplement 2A and 2B**). As CMT2D mutation within R280H not only reduces microtubule binding affinity
229 and transport but also impacts binding to SFPQ, this pathologic mutation is likely to disproportionately
230 affect transport of the RNA cargo transported together with SFPQ.

231 To model axon degeneration induced by KIF5A mutation in R280H *in vitro*, we expressed the KIF5A
232 R280H mutation by lentivirus in DRG sensory neurons that also express the endogenous WT KIF5A. As
233 observed in patients heterozygous for CMT2D mutations, overexpression of R280H led to axon
234 degeneration in DRG sensory neurons (**Figure 6E and 6F**), while control studies indicate that
235 overexpression of WT does not compromise axon integrity (**Figure 6E and 6F**). This model provides a
236 platform for investigating the molecular changes that cause degeneration in CMT disease.

237

238 **Axon degeneration caused by CMT2D R280H KIF5A mutation can be rescued by a Bclw mimetic peptide.**

239 KIF5A motors are involved in transport of mitochondria, vesicles, and other membrane enclosed
240 organelles as well as RNA granules; thus degeneration of axons caused by R280H KIF5A mutation could
241 be a consequence of defect in transport of any or all of these cargos. A similar pattern of axon
242 degeneration is observed in sensory neurons expressing the SFPQ Y527A mutant, suggesting that SFPQ-
243 RNA granules may represent a critical cargo impacted in CMT patients with KIF5A R280H mutations. Local

244 translation of mRNAs bound to SFPQ is a critical step that promotes axon survival; *bclw* is one such mRNA
245 that is bound by SFPQ and is translated in axons of DRG sensory neurons (**Figure 7A**). We asked whether
246 restoring functions downstream of the SFPQ pathway can rescue degeneration caused by KIF5A R280H
247 mutant. Intriguingly, a BH4 peptide mimetic of Bclw introduced into axons of R280H KIF5A mutant can
248 prevent axon degeneration in this genetic model of CMT with axonal survival returning to the levels
249 observed in control or WT KIF5A overexpressing DRG neurons (**Figure 7B**). This effect is specific to Bclw
250 since introducing a peptide mimetic of related Bcl2 proteins did not prevent degeneration, and
251 degeneration remained at the level observed with the R280H mutant alone (**Figure 7C**). Taken together,
252 these data suggest that defective transport of SFP-RNA granules containing *bclw* mRNA represents a key
253 mechanism that underlies CMT2D-causing mutations of KIF5A, and so causes axon degeneration.

254

255 **Discussion**

256 Kinesins are a large family of microtubule-dependent motors that play a pivotal role in rapid
257 intracellular transport. These motors are particularly critical in neurons that form extensive axonal and
258 dendritic projections and so rely on fast transport across long distances. While mutations in kinesin motors
259 cause neurodegenerative diseases affecting primary sensory and motor neurons, it is not known whether
260 this reflects a requirement for specific kinesins in mediating transport of particular cargos within the
261 lengthy axons that extend to peripheral targets, or whether degeneration reflects a more global loss of
262 axonal transport. Here we show that the non-membrane enclosed RNA granules containing the RNA
263 binding protein SFPQ selectively and directly interact with kinesin containing the KIF5A heavy chain and
264 the cargo adaptor KLC1. Therefore, mutations in KIF5A that cause sensory neuropathy preferentially
265 impact motility of SFPQ granules that transport *bclw* and other mRNAs, and the degeneration caused by
266 KIF5A mutations can be prevented by a peptide that mimics the function of the locally translated protein
267 Bclw.

268 Although it is widely accepted that RNA-granules are non-membrane enclosed organelles that
269 move by microtubule-dependent transport, how such RNA-granules associate with motors and move
270 through the axoplasm is not yet known. Our data demonstrate a direct interaction between SFPQ and the
271 kinesin-1 cargo adaptor complex KLC1, and we show that this interaction is required for autonomous
272 axonal transport. In contrast to this direct transport system, a recent study by Liao *et al.* demonstrated
273 that RNA-granules containing β -actin mRNA rely on annexin A11 adaptor protein to hitchhike on
274 lysosomes and thereby regulate growth cone morphology (Liao et al., 2019). As SFPQ does not bind β -
275 actin but instead binds mRNAs that promote axonal survival, our findings indicate that distinct pools of
276 RNA-granules containing different mRNAs rely on divergent modes of axonal transport.

277 Data from quantitative mass spectrometry and isothermal titration calorimetry demonstrate that
278 SFPQ preferentially binds KLC1/KIF5A in DRG sensory neurons and that an evolutionarily conserved Y-
279 acidic motif is sufficient for binding directly to KLC1. Interestingly, binding of the protein cargo/adaptors
280 JIP1, TorsinA and SH2D6 to KLC1 require Y-acidic motifs within an unstructured part of the molecule
281 (Nguyen et al., 2018; Pernigo et al., 2018), whereas the motif within SFPQ resides in the highly structured
282 coiled-coil region of SFPQ (**Figure 4A and Figure 4-figure supplement 1**). As RNA interactions enable SFPQ
283 to bind KIF5A/KLC1, formation of a RNP complex may expose the Y-acidic motif within the coiled-coil
284 domain. Thus, the structural basis for the interaction of KIF5A/KLC1 with SFPQ-RNA granules is likely to
285 differ from the mechanism for binding of KIF5A/KLC1 to JIP1. Consistent with this distinction, the N343S
286 mutation of KLC1 that disrupts interaction with JIP1 (Pernigo et al., 2018; Zhu et al., 2012) has no effect
287 on binding with SFPQ (**Figure 5-figure supplement 1B**). Instead the highly divergent C-terminal region of
288 KLC1 affects binding to SFPQ (**Figure 3D-F**). As the carboxy terminal region of KLC1 diverges among several
289 splice variants of KLC1 (McCart, Mahony, & Rothnagel, 2003), individual isoforms of KLC1 that are present
290 in DRG sensory neurons may specify binding to SFPQ-RNA granules.

291 Similar to other phase separating RBPs, SFPQ contains an intrinsically disordered region in its N-
292 terminal region (**Introduction-figure supplement 1**) and SFPQ assembles into large RNA transport
293 granules, which are non-membrane enclosed organelles (Kanai et al., 2004). In the nucleus, SFPQ interacts
294 with members of the DBHS proteins, NONO and PSPC1, and also binds RNA fragments of NEAT1_2 in order
295 to form paraspeckle nuclear bodies, another phase separating structure (Yamazaki et al., 2018). As is the
296 case for paraspeckle formation, RNA is a critical component of transport granules; RNase treatment leads
297 to loss of integrity of these axonal granules (Knowles et al., 1996), and binding between SFPQ and
298 KIF5A/KLC1 is highly sensitive to RNase treatment (**Figure 3A-C**). Binding to mRNAs such as *bclw* may
299 induce a conformational change in SFPQ that facilitates oligomerization and phase separation and exposes
300 the Y-acidic motif within the coiled coil domain so it can bind KLC1/KIF5A. Further structural studies
301 investigating how specific RNA cargos regulate the conformation and binding of SFPQ to KLC1 and KIF5A
302 will be necessary to fully evaluate this hypothesis.

303 Among the three *KIF5* genes encoding the kinesin-1 family of motors, the *KIF5A* gene is the only
304 one associated with the human neurological diseases CMT2D, HSP and ALS. Our results demonstrate that
305 binding of SFPQ to KLC1 complexed with KIF5A rather than KIF5B or KIF5C enables transport of SFPQ-RNA
306 granules and promotes axon survival. Based on these findings, we postulate that defective transport of
307 SFPQ-RNA granules is a major contributor to KIF5A-associated neurodegenerative disorders, rather than
308 axon degeneration in these disorders being the result of a generalized impairment of transport.

309 SFPQ RNA-granules are critical for development and maintenance of axons in motor neurons as
310 well as in sensory neurons; and human mutations in *SFPQ* and *KIF5A* have been implicated in ALS (Thomas-
311 Jinu et al., 2017). Interestingly, the Y527 residue of the Y-acidic motif lies adjacent to the two identified
312 ALS mutations: N533H and L534I; these two mutations lead to defects in the axonal functions of SFPQ in
313 motor neurons (Thomas-Jinu et al., 2017) and our data suggest that this may reflect altered binding of
314 SFPQ to KIF5A/KLC1 and altered autonomous transport of these non-membrane enclosed granules.

315 Moreover, ALS-associated mutations in *KIF5A* transform the C-terminal region of the protein (Nicolas et
316 al., 2018), the domain required for SFPQ binding. Therefore, altered binding and axonal transport of SFPQ
317 may explain the axon degeneration of motor neurons in patients harboring ALS-associated mutations in
318 *SFPQ* or *KIF5A*. A recent study by Luisier *et al.* demonstrated that aberrant localization of SFPQ is also a
319 molecular hallmark of multiple familial and sporadic models of ALS that do not exhibit mutations in *SFPQ*
320 or *KIF5A* (Luisier et al., 2018), suggesting that disrupted transport and axonal function of SFPQ may
321 contribute to additional neurodegenerative disorders. Here we demonstrated that a Bclw peptide
322 mimetic rescues axon degeneration caused by R280H *KIF5A* mutations (**Figure 7**), extending previous
323 evidence that this therapeutic approach prevents paclitaxel-induced axon degeneration (Pease-Raissi et
324 al., 2017). Taken together, our data suggests that Bclw peptide mimetics should be explored as a potential
325 therapeutic intervention for preventing axon degeneration in multiple neurological diseases that share
326 defects in RNA transport as part of their pathophysiology.

327 **Acknowledgments**

328 We thank Thomas Schwarz and Himanish Basu (Boston Children's Hospital, MA) for Kymolyzer software.
329 We thank Gary Banker (Oregon Health and Science University, OR) and Marvin Bentley (Rensselaer
330 Polytechnic Institute, NY) for *KIF5A*, *KIF5B*, *KIF5C* and *KLC1* constructs; and Corinne Houart (Kings's College
331 London, United Kingdom) for SFPQ construct. We thank the Segal lab, Charles Stiles and Michael
332 Greenberg for helpful comments on this manuscript.

334 **Declaration of Interests**

335 R.A.S. family member is on BoD for Allergen; SAB member for Amgen and Decibel Therapeutics. L.D.W. is
336 a stockholder in Aileron Therapeutics. J.A.M. receives sponsored research funding from Vertex and
337 AstraZeneca and serves on the SAB of 908 Devices.

338 **Material and Methods**

339

340 **Table for Reagents and Resources**

REAGENT or RESOURCE	SOURCE	IDENTIFIER
Antibodies		
rabbit polyclonal anti-KIF5A; WB, IF	Abcam	ab5628
rabbit polyclonal anti-KIF5B; WB, IF	Abcam	ab5629
rabbit polyclonal anti-KIF5C; WB, IF	Abcam	ab5630
mouse monoclonal anti-SFPQ [B92]; IP	Abcam	ab11825
mouse monoclonal anti-SFPQ; WB	Sigma	WH0006421M2
KLC1 antibody [H75]; WB	Santa Cruz	sc-25735
KLC2 antibody; WB	Proteintech	17668-1-AP
Pan-Actin (D18C11) Rabbit mAb; WB	Cell Signaling	8456S
Normal Mouse IgG; IP	Millipore Sigma	12-371
Normal Rabbit IgG; IP	Cell Signaling	2729S
c-Myc Antibody (9E10); WB	Santa Cruz	sc-40
Anti-Myc Antibody; IP	Millipore Sigma	06-340-MI
Monoclonal ANTI-FLAG M2 antibody (M2); WB	Sigma	F1804
HA Tag Monoclonal Antibody (2-2.2.14); WB and IP	Thermo Fisher	26183
Anti-GFP, N-terminal antibody, WB	Sigma	G1544
Goat Anti-Rabbit IgG (H+L)-HRP conjugate; WB	Bio-Rad	1721019
Goat Anti-mouse IgG (H+L)-HRP conjugate; WB	Bio-Rad	1706516
Mouse Purified anti-Tubulin β 3 (TUBB3) Antibody; IF	Biolegend	801213
Rabbit Purified anti-Tubulin β 3 (TUBB3) Antibody; IF	Biolegend	802001
Goat anti-Mouse IgG (H+L) Alexa Fluor 488; IF	Invitrogen	A-11001
Goat anti-Rabbit IgG (H+L) Alexa Fluor 546; IF	Invitrogen	A-11010
Donkey anti-Mouse IgG (H+L) Alexa Fluor 488	Invitrogen	A-21202
Donkey anti-Mouse IgG (H+L) Alexa Fluor 647	Invitrogen	A-31573
Bacterial and Virus Strains		
shSFPQ	Sigma	TRCN0000102240
shKIF5A	Sigma	TRCN0000415243
shKIF5C	Sigma	TRCN0000090857
Chemicals, Peptides, and Recombinant Proteins		
ESEMEDAYHEHQANLLR (SFPQ WT)	KE Biochem	Custom
ESEMEDAAHEHQANLLR (SFPQ Y527A)	KE Biochem	Custom
Bclw BH4 SAHB _A	Loren D. Walensky	Walensky Laboratory, Dana-Farber Cancer Institute
Bcl2 BH4 SAHB _A	Loren D. Walensky	Walensky Laboratory, Dana-Farber Cancer Institute
Puromycin dihydrochloride	Sigma	P9620
Rnase A/T1 Mix	Thermo Fisher	FEREN0551
FuGENE 6 Transfection Reagent	Promega	E2691
Lipofectamine 2000 Transfection Reagent	Invitrogen	11668027
In-Fusion HD Cloning Plus	Clontech	638909
Q5 Site-Directed Mutagenesis Kit	New England BioLabs	E0554S
cOmplete, Mini, EDTA-free protease inhibitor cocktail	Millipore Sigma	11836170001

Halt Phosphatase inhibitor cocktail	Thermo Scientific	78420
Amersham ECL western blotting detection system	VWR	95038-570
SuperSignal West Dura Extended Duration Substrate	Thermo Scientific	34076
Dynabeads protein G	Invitrogen	10003D
Sera-Mag Carboxylate-Modified Magnetic Particles	GE Healthcare	24152105050250
Neurobasal Medium	Gibco	21103049
Neurobasal Medium, minus phenol red	Gibco	12348017
Hibernate E Low Fluorescence	Brain Bits	HELF500
B-27 Supplement, serum free	Gibco	17504044
GlutaMAX Supplement	Gibco	35050061
DMEM, high glucose, pyruvate	Gibco	11995065
Fetal Bovine Serum	Corning cellgro	B003L51
Corning Matrigel GFR Membrane Matrix	Fisher Scientific	CB40230C
Laminin Mouse Protein, Natural	Gibco	23017015
Poly-D-lysine hydrobromide	Sigma	P6407
Recombinant Human β -NGF	Peprtech	450-01
Recombinant Human/Murine/Rat BDNF	Peprtech	450-02
tetramethyl Rhodamine (TMR)	Promega	G8251
Chariot protein delivery system	Active Motif	30025
Critical Commercial Assays		
Amicon Ultra-15 Centrifugal Filter Units	Millipore Sigma	UFC910024
NuPAGE 4-12% Bis-Tris Protein Gels, 1.0mm, 10 well	Thermo Fisher	NP0321
450 μ m microgroove barrier silicone device	Xona Microfluidics	SND450
900 μ m microgroove barrier XonaChips	Xona Microfluidics	XC900
Poly-d-lysine solution optimized for Xona platforms	Xona Microfluidics	XonaPDL
Teflon Divider chamber, 20mm OD	Tyler Research	CAMP10
Experimental Models: Cell Lines		
Human HEK 293T	ATCC	CRL-3216
Experimental Models: Organisms/Strains		
Sprague Dawley Rat	Charles River Laboratory	N/A
Recombinant DNA		
FUGW	(Lois, Hong, Pease, Brown, & Baltimore, 2002)	Addgene #14883
pLV-EF1a-IRES-Puro	(Hayer et al., 2016)	Addgene #85132
pMD2.G	Didier Trono	Addgene #12259
pxPAX2	Didier Trono	Addgene #12260
UbC-Halo-SFPQ	This paper	N/A
pLV-EF1a-GFP-SFPQ-IRES-mCherry	This paper	N/A
pLV-EF1a-GFP-SFPQ (Y527A)-IRES-mCherry	This paper	N/A
pLV-EF1a-KIF5A-HA-IRES-Puro	This paper	N/A
pLV-EF1a-KIF5A(R280H)-HA-IRES-Puro	This paper	N/A
FLAG-KIF5A	This paper	N/A
FLAG-KIF5A Δ tail	This paper	N/A
FLAG-KIF5A (R280H)	This paper	N/A
HA-KIF5A	This paper	N/A
HA-SFPQ	This paper	N/A

FLAG-SFPQ	This paper	N/A
FLAG-SFPQ (Y527A)	This paper	N/A
KLC1-Myc	This paper	N/A
KLC1-Myc (N343S)	This paper	N/A
Myc-KLC1	This paper	N/A
Myc-KLC1 Δtail	This paper	N/A
hsSFPQ pcS2	(Thomas-Jinu et al., 2017)	N/A
pBa-GFP-Inkr-mmKIF5a	Gary Banker and Marvin Bentley	N/A
pBa-GFP-mmKIF5B	Gary Banker and Marvin Bentley	N/A
pBa-mCherry-myc-KIF5C	Gary Banker and Marvin Bentley	N/A
pBa-GFP-3myc-mmKLC1a	Gary Banker and Marvin Bentley	N/A
pET28MHL-hsKLC1 (205-501)	Cheryl Arrowsmith	Addgene #26096
Software and Algorithms		
(Fiji is just) ImageJ 2.0.0	NIH	http://imagej.nih.gov/ij
Prism7	GraphPad Software	https://graphpad.com/
NIS-Elements Imaging Software	Nikon	https://www.healthcare.nikon.com/en/
NanoAnalyze Software	TA instruments	https://www.tainstruments.com/support/software-downloads-support/downloads/
Kymolyzer	(Shlevkov et al., 2019)	N/A

341
342 All experimental procedures were done in accordance with the National Institute of Health guidelines and
343 were approved by the Dana-Farber Cancer Institutional Animal Care and Use Committee.

344
345 Animal Use: Time pregnant Sprague-Dawley rats were purchased from Charles River.

346
347 DNA and shRNA constructs: Constructs used for HEK 293T IP studies were cloned into pcDNA3.1 vector
348 using PCR-based In-Fusion HD cloning (Clontech). KIF5 (pBa-GFP-Inkr-mmKIF5A; pBa-GFP-mmKIF5B; pBa-
349 mCherry-myc-KIF5C) and KLC1 (pBa-GFP-3myc-mmKLC1a) constructs were a gift from Dr. Garry Banker
350 and Dr. Marvin Bentley and were used as a template to clone HA, FLAG or Myc-tagged constructs: HA-
351 KIF5A, FLAG-KIF5A (WT, Δtail, and R280H), KLC1-Myc (WT and N343S) and Myc-KLC1 (WT and Δtail).
352 Human version of SFPQ (hsSFPQ pcS2) was a gift from Dr. Corinne Houart and was used to clone HA and
353 FLAG-tagged constructs: HA-SFPQ, and FLAG-SFPQ (WT and Y527A). The R280H KIF5A, N343S KLC1 and
354 Y527A SFPQ mutants were generated by Q5 site-directed mutagenesis (NEB) using manufacturer's
355 instructions. Lentiviral constructs used for compartmented Campenot cultures were cloned into pLV-
356 EF1a-IRES-Puro, a gift from Tobias Meyer (Addgene plasmid #85132), for KIF5A-HA (WT and R280H) or
357 into pLV-EF1a-IRES-mCherry for GFP-SFPQ (WT and Y527A). For live cell imaging of SFPQ, Halo-tagged
358 SFPQ was cloned into FUGW, a gift from David Baltimore (Addgene plasmid #14883), as a backbone vector.
359 The shRNAs against shSFPQ (TRCN0000102240), KIF5A (TRCN0000415243) and KIF5C (TRCN0000090857)
360 were purchased from Mission.

361 DRG sensory neuron culture: DRGs from embryonic day 15 rats of either sex were dissected and
362 trypsinized. For mass cultures, 300,000 cells were plated onto p35 dishes coated with Corning Matrigel
363 GFR Membrane Matrix (Thermo Fisher) diluted in DMEM (Thermo Fisher). Cultures were maintained in
364 Neurobasal (Invitrogen) with 2% B27 supplement (Invitrogen), 1% Penicillin/streptomycin, 1% GlutaMAX
365 (Life Technologies) and 0.08% glucose at 37°C and 7.5% CO₂. DRG neurons were plated with 0.3 μM AraC;
366 100 ng/mL NGF (Peprotech) + BDNF (Peprotech); and on DIV2 neurotrophins were reduced to 10 ng/mL
367 NGF + BDNF with AraC and maintained until DIV6 for collection and lysis.

368 For compartmented Campenot chambers, 120,000 cells were plated in the cell body compartment of a
369 Teflon divider (Camp10, Tyler Research) attached to a p35 dish coated with Corning Matrigel GFR
370 Membrane Matrix diluted in DMEM. DRG neurons were initially plated with 0.3 μM AraC; 100 ng/mL
371 NGF + BDNF; and on DIV1 neurotrophins were reduced to 10 ng/mL NGF + BDNF with AraC only in the cell
372 body compartment. On DIV2 cultures were maintained in the same neurotrophin concentration (10 ng/mL
373 for cell body and 100 ng/mL for distal axons) but without AraC and reduced to 0 ng/mL NGF + BDNF in the
374 cell body compartment and 1 ng/mL NGF + BDNF in the distal axon compartment with AraC from DIV5 to
375 DIV8 for collecting protein lysates or for degeneration assay. As efficient knockdown of SFPQ with shRNA
376 takes up to DIV8, the Campenot cultures used for degeneration assay involving shSFPQ were maintained
377 until DIV12 with the following modifications: from DIV5 to DIV8, neurotrophins were maintained at
378 10 ng/mL NGF + BDNF for both cell body and axons with AraC and then reduced to 1 ng/mL NGF + BDNF
379 for both cell body and axons with AraC until DIV12.

380 Microfluidic device with 900 μm microgroove barrier XonaChip (XC900; Xona) was prepared for live cell
381 imaging following manufacturer's instructions except following the PBS washes for XonaPDL (Xona)
382 coating, the device was further incubated with 10 μg/mL of laminin (Life Technologies) for 3 hours at 37°C.
383 The device was then washed with PBS and primed with DRG neuron media until plating. In the cell body
384 compartment, 20,000 DRG neurons (dissected out from embryonic day 14 rats) were plated to attach at
385 room temperature for 5 min. DRG neurons were infected with lentivirus in the cell body compartment
386 diluted in media containing 0.3 μM AraC; 100 ng/mL NGF + BDNF and fresh media with 0.3 μM AraC;
387 100 ng/mL NGF + BDNF added to the distal axon compartment. At DIV1, virus was removed and replaced
388 with fresh media to both compartments with the cell body neurotrophins reduced to 10 ng/mL NGF +
389 BDNF with AraC and distal axon compartment with 0.3 μM AraC; 100 ng/mL NGF + BDNF. At DIV2, both
390 cell body and distal axon compartment were kept in 0.3 μM AraC; 5 ng/mL NGF + BDNF until live cell
391 imaging at DIV5.

392 For immunofluorescence in microfluidic chambers, silicon-based 450μm microgroove barrier (SND450;
393 Xona) was prepared following manufacturer's instructions with modifications. Sterilized cover glass was
394 coated with 0.2 mg/mL poly-D-lysine (Sigma) overnight, then washed with water and dried. Microfluidic
395 chambers were cleaned by briefly soaking it in ethanol then dried; attached onto PDL-coated glass slide;
396 and the chambers and the wells were filled with 10 ug/mL laminin and incubated for 3 hours at 37°C. The
397 chambers and wells were washed three times with neurobasal media and 30,000 DRG neurons were
398 plated in the cell body compartment with 0.3 μM AraC; 50 ng/mL NGF + BDNF and 0.3 μM AraC;
399 100 ng/mL NGF + BDNF in the distal axon compartment. At DIV1, both compartments were replaced with
400 fresh media with 0.3 μM AraC; 10 ng/mL NGF + BDNF in the cell body compartment and 0.3 μM AraC;
401 100 ng/mL NGF + BDNF in the distal axon compartment and maintained until DIV5 for immunostaining.
402 See Fenstermacher *et al.* for more details on compartmented culture system (Fenstermacher, Pazyra-
403 Murphy, & Segal, 2015).

404 Axonal degeneration assay: Compartmented chamber cultures were fixed at room temperature with 4%
405 PFA diluted 1:2 in DRG neuron media for 10 min, then an additional 20 minutes in undiluted 4% PFA. DRGs
406 were permeabilized with 0.1% Triton X-100 for 10 min; blocked in 3% BSA in 0.1% Triton X-100 for 1 hour
407 at room temperature; and incubated with rabbit anti-Tuj1 (1:400; Biolegend) overnight at 4°C. Cultures
408 were then incubated with secondary antibodies (1:1000; Invitrogen) for 1 hour at room temperature and
409 stained briefly with DAPI. Images of distal axon tips were obtained using a 40X air objective, and axonal
410 degeneration was quantified as a degeneration index, as previously described (Cosker et al., 2016; Sasaki,
411 Vohra, Lund, & Milbrandt, 2009). For peptide rescue experiment, the following peptides synthesized as
412 previously described (Barclay et al., 2015; Pease-Raissi et al., 2017) were used:

413 Bclw BH4 SAHB_A ALVADFGYKLRXKGYXBGA

414 Bcl2 BH4 SAHB_A EIVBKYIHYKLSXRGYXWDA

415 (differential placement of all-hydrocarbon staples (X) along the BH4 sequences of Bclw and Bcl2; and B
416 represents norleucine, replacing the native cysteine and methionine on Bclw and Bcl2, respectively)

417 The peptides were introduced into axons using 2 µL Chariot protein transfection system (Active Motif)
418 only in the distal axon compartment of compartmented Campenot chambers immediately after R280H
419 virus removal at DIV2. The culture was kept with the peptides until DIV8 for axon degeneration assay.

420 Immunofluorescence: DRG neurons grown in silicon-based microfluidic chambers were fixed with 4% PFA
421 in PBS for 20 minutes at room temperature then washed three times with PBS. The device was then
422 carefully removed and then cultures were immediately permeabilized with 0.1% triton in PBS for 10
423 minutes at room temperature and blocked for 1 hour at room temperature with 3% BSA in PBS. KIF5
424 primary antibodies (1:100; abcam) and mouse TUJ1 (1:400; Biolegend) diluted in 3% BSA in PBS were
425 incubated at 4°C overnight. The slides were washed three times with PBS and secondary antibodies diluted
426 in 3% BSA in PBS (1:1000; Invitrogen) were incubated for 1 hour at room temperature. Finally, the slides
427 were washed two times with PBS and incubated with DAPI (1:1000) in PBS; washed briefly and mounted.
428 Images were acquired with Nikon C2 Si laser-scanning confocal microscope with 60x oil objective using
429 NIS-Elements imaging software.

430 Whole mount immunostaining: Whole DRG with peripheral nerves were dissected from P1 mice of either
431 sex and fixed with 4% PFA at 4°C overnight. DRGs were washed in PBS, permeabilized in 0.5% Triton X-
432 100 for 1 hour and blocked in 5% BSA and 0.5% Triton X-100 for 4 hours. DRGs were incubated for 48
433 hours in primary KIF5 (1:50, Abcam) and TUJ1 (1:300, Biolegend) antibodies at 4°C and washed overnight
434 in PBS. DRGs were then incubated in secondary antibody (1:500; Life Technologies) at room temperature
435 for 3.5 hours. Images were acquired with Nikon C2 Si laser-scanning confocal microscope with 40x oil
436 objective.

437 Live cell imaging: DRGs neurons infected with lentivirus expressing Halo-SFPQ were grown in XonaChip
438 microfluidic chambers and were labeled with tetramethyl Rhodamine (TMR) Halo Tag ligand (Promega)
439 according to the manufacturer's instructions with modifications. TMR stock was diluted in DRG culture
440 media at 1:200 and used at a final labeling concentration of 2.5 µM added to both cell body and axon
441 compartment. DRGs were incubated for 15 mins at 37°C and washed 3 times with complete culture media
442 made with neurobasal without phenol red and incubated for 30 mins at 37°C to wash unbound ligand.
443 DRG culture media was replaced with low fluorescence imaging media (HibernateE; Brain Bits)
444 supplemented with 2% B27 and 1% GlutaMAX. DRG neurons were imaged live in an environmental
445 chamber at 37°C and 7.5% CO₂ using a 60x oil 1.4NA objective with a Perfect Focus System one frame
446 every 1.5 sec for 3 mins. Images were analyzed using Kymolyzer macro for ImageJ developed by the

447 laboratory of Dr. Thomas Schwarz (Shlevkov et al., 2019). To determine the SFPQ granule diameter,
448 measurement was taken from the two edges of the granule running parallel to the direction of the axon.

449 Western blot: HEK 293T cells or DRG sensory neurons were collected and prepped with lysis buffer (1%
450 NP-40; 50mM Tris-HCl, pH 7.4; 150mM NaCl; 2mM EDTA; protease inhibitor (Sigma); and phosphatase
451 inhibitor (Life Technologies)). Cell lysates were placed on ice for 20 minutes and centrifuged at 13,000
452 rpm for 20 minutes to collect the supernatant. The lysates were separated by 4-12% Bis-Tris NuPAGE gel
453 (Thermo Fisher) and blotted with the following primary antibodies: mouse anti-SFPQ (1:1000; Sigma),
454 rabbit anti-KIF5A (1:2000; Abcam), rabbit anti-KIF5B (1:2000; Abcam), rabbit anti-KIF5C (1:2000; Abcam),
455 rabbit anti-KLC1 (1:500; Santa Cruz), rabbit anti-KLC2 (1:1000; Proteintech), rabbit anti-pan actin (1:1000;
456 Cell Signaling), mouse anti-Myc (1:500; Santa Cruz), mouse anti-FLAG (1:1000; Sigma), mouse anti-HA
457 (1:10,000; Thermo Fisher), rabbit anti-GFP (1:2000; Sigma). HRP-conjugated secondary antibodies
458 (1:10,000; BioRad); ECL detection system (VWR) and SuperSignal West Dura (Thermo Fisher) were used
459 for chemiluminescent detection.

460 Transfection and immunoprecipitation: HEK 293T cells were cultured in a 10 cm plate with DMEM, 10%
461 FBS (Thomas Scientific) and 1% Penicillin/streptomycin at 37°C and 5% CO₂. For transfection, cells were
462 plated in a 6 cm dish and 24 hours later plasmids were transfected with Lipofectamine 2000 (Invitrogen)
463 based on manufacture's protocol and then incubated for 24 hours before immunoprecipitation
464 experiments.

465 For immunoprecipitation, HEK 293T cell or DRG neurons were collected and lysed as described for western
466 blots, and 500 µg of protein lysate was precleared with 3 µL of Dynabeads protein G (Thermo Fisher) for
467 1 (HEK 293T lysates) or 2 hours (DRG neuron lysates) nutated at 4°C. For RNase experiments, the lysate
468 was treated with RNase A/T1 (Fisher Scientific) for 1 hour at room temperature and immediately
469 immunoprecipitated. Following the manufacturer's instructions, protein lysate was immunoprecipitated
470 for 2 hours at 4°C with the following antibodies: rabbit anti-myc (2.5 µg, Millipore Sigma), mouse anti-HA
471 (2.5 µg, Thermo Fisher), mouse anti-SFPQ (20 µg, Abcam), control normal mouse (Millipore Sigma) or
472 normal rabbit IgG (Cell Signaling),. The input (0.5% for HEK 293T and 3% for DRG) and the elute was
473 analyzed by western blot.

474 Lentivirus production and infection: HEK 293T cells grown on 10 cm dish were transfected using FuGENE
475 6 (Promega) with the transfer vector pXPA2 (Addgene #12260) and pMD2.G (Addgene plasmid #12259),
476 gifts from Didier Trono, at a ratio of 4:3:1. The transfection reagent was replaced with fresh media after
477 24 hours. Virus-containing media were collected 48- and 72-hours post transfection; pooled; centrifuged
478 at 1200 rpm for 5 minutes; and filtered through a 0.45 µm PES filter. Finally, the virus was concentrated
479 using Amicon ultra-15 centrifugal filter units (Millipore Sigma) by centrifuging at 3000 rpm and stored at
480 -80°C until use. For infection of DRG sensory neurons, virus was added at DIV1 for 24 hours, except for
481 XonaChip where virus was added immediately after plating. For experiments involving puromycin (Sigma)
482 selection (Figure 6D, shSFPQ; Figure 6F, KIF5A WT and R280H constructs; Figure 2-figure supplement 1C
483 and 1D, shKIF5A and shKIF5C; Figure 6-figure supplement 1, shSFPQ), the neurons were allowed to recover
484 for 1 day after virus removal and 0.4 µg/mL puromycin was then added at DIV3 and replaced with fresh
485 media at DIV5.

486
487 Protein expression and purification: A construct of human KNS2 covering residues 205-501 in the
488 pET28MHL vector, a gift from Cheryl Arrowsmith (Addgene plasmid #26096) was expressed in E. coli BL21
489 (DE3) in TB medium in the presence of 50 µg/mL of kanamycin. Cells were grown at 37°C to an OD of 0.6,
490 induced overnight at 17°C with 400 µM isopropyl-1-thio-D-galactopyranoside, collected by centrifugation,

491 and stored at -80°C. Cell pellets were microfluidized at 15,000 psi in buffer A1 (25mM HEPES (7.5), 500mM
492 NaCl, 5% glycerol, 30mM Imidazole, 5uM ZnAc, and 7mM BME) and the resulting lysate was centrifuged
493 at 13,000 rpm for 40 min. Ni-NTA beads (Qiagen) were mixed with lysate supernatant for 45 min, washed
494 with buffer A1, and eluted with buffer Bi (25mM HEPES (7.5), 500mM NaCl, 5% glycerol, 400mM Imidazole,
495 5uM ZnAc, and 7mM BME). The sample was gel-filtered through a Superdex-200 16/60 column in buffer
496 A3 (20mM HEPES (7.5), 200mM NaCl, 5% glycerol, 1mM DTT, and 0.5mM TCEP). Fractions were pooled,
497 but protein began precipitating when concentrated. To combat apparent precipitation, excess NaCl
498 solution was added to a final buffer composition of 18mM HEPES-7.5, 680mM NaCl, 4.5% glycerol, 0.9mM
499 DTT, and 0.45mM TCEP. Adjusted sample was then concentrated and stored at -80°C.

500
501 Isothermal Titration Calorimetry (ITC): All calorimetric experiments were carried out in 20mM HEPES, pH
502 7.5, 150mM NaCl, and 0.5mM TCEP, with 2% DMSO at 25°C using an Affinity ITC from TA Instruments
503 (New Castle, DE) equipped with auto sampler. Briefly, 350µL of buffer or protein at 20µM was placed into
504 the calorimetric cell, and 250µL of various SFPQ peptides (KE BioChem) at 200µM were loaded into
505 titration syringe. 4µL syringe solution was injected into the calorimetric cell 30 times with a 200 second
506 interval between injections. Thermodynamic parameters (Kd, stoichiometry, and enthalpy) were
507 calculated according to the single site model provided in NanoAnalyze software (TA instruments).

508
509 Mass Spectrometry: Antibody-conjugated protein G beads from KLC1 and SFPQ immunoprecipitates were
510 suspended in 100 µL of ammonium bicarbonate, reduced with 10 mM dithio-treitol (DTT) for 30 minutes
511 at 56°C and alkylated with 20 mM iodoacetamide for 20 minutes at 22°C in the dark. Excess iodoacetamide
512 was quenched by adding 10 mM dithio-treitol (DTT) before diluting the samples to 250 µL with 100 mM
513 ammonium bicarbonate. Immunoprecipitated proteins were digested overnight at 37°C with 4 µg of
514 trypsin. Tryptic peptides were desalted using 500 µg of a 1:1 mixture of hydrophobic and hydrophilic Sera-
515 Mag Carboxylate-modified Speed Beads (GE Healthcare Life Sciences).

516
517 Peptides were loaded onto a precolumn (100 µm × 4 cm POROS 10R2, Applied Biosystems) and eluted
518 with an HPLC gradient (NanoAcquity UPLC system, Waters; 1%–40% B in 90 min; A = 0.2 M acetic acid in
519 water, B = 0.2 M acetic acid in acetonitrile). Peptides were resolved on a self-packed analytical column (30
520 µm × 50 cm Monitor C18, Column Engineering) and introduced in the mass spectrometer (QExactive HF
521 mass spectrometer, ThermoFisher Scientific) equipped with a Digital PicoView electrospray source
522 platform (New Objective)(Ficarro et al., 2009).

523
524 The mass spectrometer was programmed to perform a combination of targeted (Parallel Reaction
525 Monitoring, PRM) and data dependent MS/MS scans. To select precursors for the PRM experiments, we
526 first analyzed a small aliquot of digested KLC1 immunoprecipitate and selected the most intense precursor
527 for peptides mapping uniquely to genes (Askenazi, Marto, & Linial, 2010) encoding each protein of interest.
528 In data-dependent mode, the top 5 most abundant ions in each MS scan were subjected to collision
529 induced dissociation (HCD, 27% normalized collision energy) MS/MS (isolation width = 1.5 Da, intensity
530 threshold = 1E5, max injection time: 50 ms). Dynamic exclusion was enabled with an exclusion duration
531 of 30 seconds. PRM scans were scheduled across an 8 minute-period for each of 45 precursors selected
532 as described above (isolation width = 1.6 Da, max injection time: 119 ms). ESI voltage was set to 3.8 kV.

533
534 MS spectra were recalibrated using the background ion (Si(CH₃)₂O)₆ at m/z 445.12 +/- 0.03 and converted
535 into a Mascot generic file format (.mgf) using multiplier scripts (Alexander, Ficarro, Adelmant, & Marto,
536 2017; Askenazi, Parikh, & Marto, 2009; Parikh et al., 2009). Spectra were searched using Mascot (version
537 2.6) against three appended databases consisting of: i) rat protein sequences (downloaded from UniProt
538 on 04/09/2018); ii) common lab contaminants and iii) a decoy database generated by reversing the

539 sequences from these two databases. Precursor tolerance was set to 20 ppm and product ion tolerance
540 to 25 mmu. Search parameters included trypsin specificity, up to 2 missed cleavages, fixed
541 carbamidomethylation (C, +57 Da) and variable oxidation (M, +16 Da). Spectra matching to peptides from
542 the reverse database were used to calculate a global false discovery rate and were discarded. Data were
543 further processed to remove peptide spectral matches (PSMs) to the forward database with an FDR
544 greater than 1.0%. Protein abundance for KLC1 and KLC2 (Fig. 1G) or KIF5A, KIF5B, KIF5C (Fig. 1H), in the
545 KLC1 immunoprecipitate was calculated by summing the extracted ion chromatogram peak area of the 3
546 most abundant (Silva, Gorenstein, Li, Vissers, & Geromanos, 2006) gene-unique peptide sequences and
547 averaged across 2 technical replicates. Due to the low absolute abundance of KLC and KIF proteins in the
548 SFPQ immunoprecipitates, we used an MS2-level quantitation approach whereby the extracted ion
549 chromatogram intensity (calculated as the area under the curve) of a set of precursor/fragment ion pairs
550 (manually selected from the targeted MS/MS experiments) in the SFPQ LC-MS/MS analyses were
551 normalized to their intensity in the KLC1 immunoprecipitate, taking into account the average abundance
552 of each KLC (Fig. 1G) or KIF5 (Fig. 1H) protein measured by the top3 quantitation method described above.

553

554 Quantification and Statistical Analysis

555 Data are expressed as mean \pm s.e.m. To assess statistical significance, data were analyzed by unpaired
556 two-tailed Student's t test. For multiple comparisons, data were analyzed by one-way ANOVA. Significance
557 was placed at $p < 0.05$. Statistical analysis was done using Microsoft Excel and GraphPad Prism.

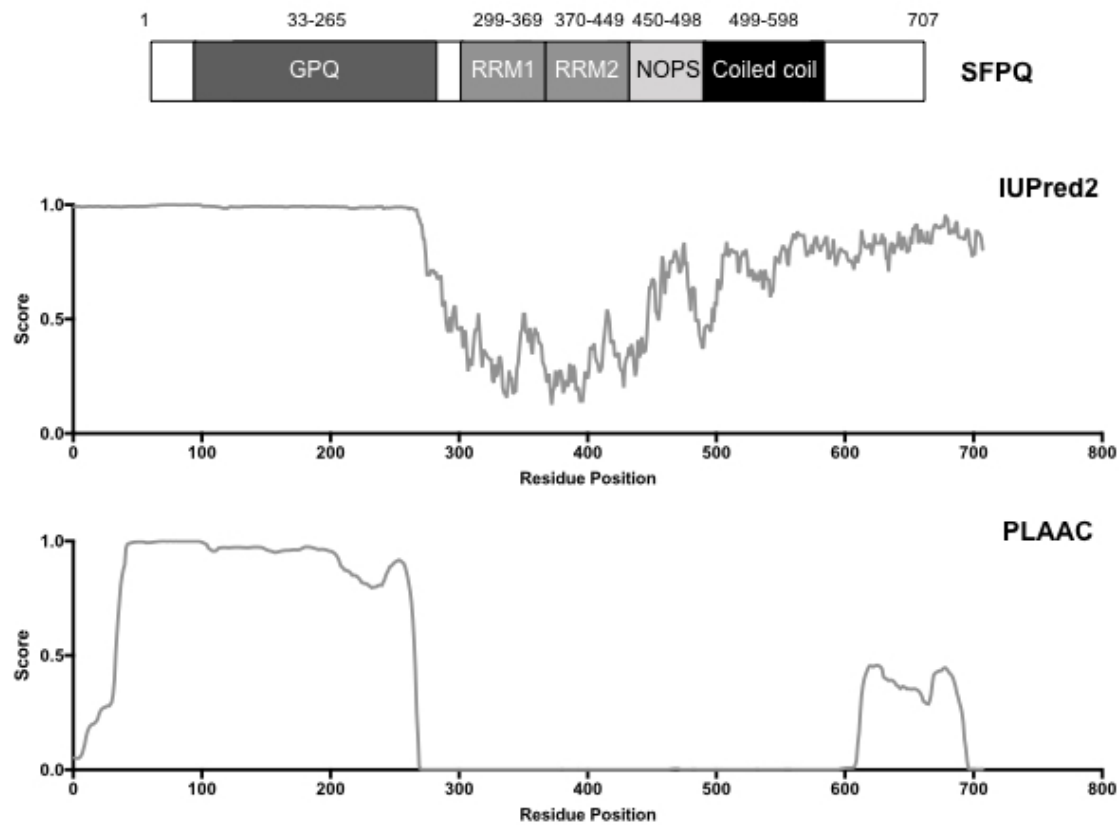
558 **References**

- 559
- 560 Alexander, W. M., Ficarro, S. B., Adelmant, G., & Marto, J. A. (2017). multipliez v2.0: A Python-
561 based ecosystem for shared access and analysis of native mass spectrometry data.
562 *Proteomics*, *17*(15-16). doi:10.1002/pmic.201700091
- 563 Askenazi, M., Marto, J. A., & Linial, M. (2010). The complete peptide dictionary--a meta-
564 proteomics resource. *Proteomics*, *10*(23), 4306-4310. doi:10.1002/pmic.201000270
- 565 Askenazi, M., Parikh, J. R., & Marto, J. A. (2009). mzAPI: a new strategy for efficiently sharing
566 mass spectrometry data. *Nat Methods*, *6*(4), 240-241. doi:10.1038/nmeth0409-240
- 567 Barclay, L. A., Wales, T. E., Garner, T. P., Wachter, F., Lee, S., Guerra, R. M., . . . Walensky, L. D.
568 (2015). Inhibition of Pro-apoptotic BAX by a noncanonical interaction mechanism.
569 *Mol Cell*, *57*(5), 873-886. doi:10.1016/j.molcel.2015.01.014
- 570 Cosker, K. E., Fenstermacher, S. J., Pazyra-Murphy, M. F., Elliott, H. L., & Segal, R. A. (2016).
571 The RNA-binding protein SFPQ orchestrates an RNA regulon to promote axon
572 viability. *Nat Neurosci*, *19*(5), 690-696. doi:10.1038/nn.4280
- 573 Das, S., Singer, R. H., & Yoon, Y. J. (2019). The travels of mRNAs in neurons: do they know
574 where they are going? *Curr Opin Neurobiol*, *57*, 110-116.
575 doi:10.1016/j.conb.2019.01.016
- 576 Dutta, M., Diehl, M. R., Onuchic, J. N., & Jana, B. (2018). Structural consequences of hereditary
577 spastic paraplegia disease-related mutations in kinesin. *Proc Natl Acad Sci U S A*,
578 *115*(46), E10822-E10829. doi:10.1073/pnas.1810622115
- 579 Ebbing, B., Mann, K., Starosta, A., Jaud, J., Schols, L., Schule, R., & Woehlke, G. (2008). Effect of
580 spastic paraplegia mutations in KIF5A kinesin on transport activity. *Hum Mol Genet*,
581 *17*(9), 1245-1252. doi:10.1093/hmg/ddn014
- 582 Fenstermacher, S. J., Pazyra-Murphy, M. F., & Segal, R. A. (2015). Campenot Cultures and
583 Microfluidics Provide Complementary Platforms for Spatial Study of Dorsal Root
584 Ganglia Neurons. In *Microfluidic and Compartmentalized Platforms for*
585 *Neurobiological Research* (pp. 105-124).
- 586 Ficarro, S. B., Zhang, Y., Lu, Y., Moghimi, A. R., Askenazi, M., Hyatt, E., . . . Marto, J. A. (2009).
587 Improved electrospray ionization efficiency compensates for diminished
588 chromatographic resolution and enables proteomics analysis of tyrosine signaling in
589 embryonic stem cells. *Anal Chem*, *81*(9), 3440-3447. doi:10.1021/ac802720e
- 590 Fuger, P., Sreekumar, V., Schule, R., Kern, J. V., Stanchev, D. T., Schneider, C. D., . . . Rasse, T. M.
591 (2012). Spastic paraplegia mutation N256S in the neuronal microtubule motor KIF5A
592 disrupts axonal transport in a Drosophila HSP model. *PLoS Genet*, *8*(11), e1003066.
593 doi:10.1371/journal.pgen.1003066
- 594 Gopal, P. P., Nirschl, J. J., Klinman, E., & Holzbaur, E. L. (2017). Amyotrophic lateral sclerosis-
595 linked mutations increase the viscosity of liquid-like TDP-43 RNP granules in
596 neurons. *Proc Natl Acad Sci U S A*, *114*(12), E2466-E2475.
597 doi:10.1073/pnas.1614462114
- 598 Hayer, A., Shao, L., Chung, M., Joubert, L. M., Yang, H. W., Tsai, F. C., . . . Meyer, T. (2016).
599 Engulfed cadherin fingers are polarized junctional structures between collectively
600 migrating endothelial cells. *Nat Cell Biol*, *18*(12), 1311-1323. doi:10.1038/ncb3438
- 601 Hewage, T. W., Caria, S., & Lee, M. (2019). A new crystal structure and small-angle X-ray
602 scattering analysis of the homodimer of human SFPQ. *Acta Crystallogr F Struct Biol*
603 *Commun*, *75*(Pt 6), 439-449. doi:10.1107/S2053230X19006599

- 604 Jennings, S., Chenevert, M., Liu, L., Mottamal, M., Wojcik, E. J., & Huckaba, T. M. (2017).
605 Characterization of kinesin switch I mutations that cause hereditary spastic
606 paraplegia. *PLoS One*, *12*(7), e0180353. doi:10.1371/journal.pone.0180353
- 607 Kanai, Y., Dohmae, N., & Hirokawa, N. (2004). Kinesin transports RNA: isolation and
608 characterization of an RNA-transporting granule. *Neuron*, *43*(4), 513-525.
609 doi:10.1016/j.neuron.2004.07.022
- 610 Knowles, R. B., Sabry, J. H., Martone, M. E., Deerinck, T. J., Ellisman, M. H., Bassell, G. J., & Kosik,
611 K. S. (1996). Translocation of RNA granules in living neurons. *J Neurosci*, *16*(24),
612 7812-7820. Retrieved from <https://www.ncbi.nlm.nih.gov/pubmed/8987809>
- 613 Liao, Y. C., Fernandopulle, M. S., Wang, G., Choi, H., Hao, L., Drerup, C. M., . . . Ward, M. E. (2019).
614 RNA Granules Hitchhike on Lysosomes for Long-Distance Transport, Using Annexin
615 A11 as a Molecular Tether. *Cell*, *179*(1), 147-164 e120.
616 doi:10.1016/j.cell.2019.08.050
- 617 Lipka, J., Kapitein, L. C., Jaworski, J., & Hoogenraad, C. C. (2016). Microtubule-binding protein
618 doublecortin-like kinase 1 (DCLK1) guides kinesin-3-mediated cargo transport to
619 dendrites. *EMBO J*, *35*(3), 302-318. doi:10.15252/embj.201592929
- 620 Liu, Y. T., Laura, M., Hersheson, J., Horga, A., Jaunmuktane, Z., Brandner, S., . . . Houlden, H.
621 (2014). Extended phenotypic spectrum of KIF5A mutations: From spastic paraplegia
622 to axonal neuropathy. *Neurology*, *83*(7), 612-619.
623 doi:10.1212/WNL.0000000000000691
- 624 Lois, C., Hong, E. J., Pease, S., Brown, E. J., & Baltimore, D. (2002). Germline transmission and
625 tissue-specific expression of transgenes delivered by lentiviral vectors. *Science*,
626 *295*(5556), 868-872. doi:10.1126/science.1067081
- 627 Luisier, R., Tyzack, G. E., Hall, C. E., Mitchell, J. S., Devine, H., Taha, D. M., . . . Patani, R. (2018).
628 Intron retention and nuclear loss of SFPQ are molecular hallmarks of ALS. *Nat*
629 *Commun*, *9*(1), 2010. doi:10.1038/s41467-018-04373-8
- 630 McCart, A. E., Mahony, D., & Rothnagel, J. A. (2003). Alternatively spliced products of the
631 human kinesin light chain 1 (KNS2) gene. *Traffic*, *4*(8), 576-580. Retrieved from
632 <https://www.ncbi.nlm.nih.gov/pubmed/12839500>
- 633 Millecamps, S., & Julien, J. P. (2013). Axonal transport deficits and neurodegenerative
634 diseases. *Nat Rev Neurosci*, *14*(3), 161-176. doi:10.1038/nrn3380
- 635 Nam, D. E., Yoo, D. H., Choi, S. S., Choi, B. O., & Chung, K. W. (2018). Wide phenotypic spectrum
636 in axonal Charcot-Marie-Tooth neuropathy type 2 patients with KIF5A mutations.
637 *Genes Genomics*, *40*(1), 77-84. doi:10.1007/s13258-017-0612-x
- 638 Nguyen, T. Q., Aumont-Nicaise, M., Andreani, J., Velours, C., Chenon, M., Vilela, F., . . . Menetrey,
639 J. (2018). Characterization of the binding mode of JNK-interacting protein 1 (JIP1) to
640 kinesin-light chain 1 (KLC1). *J Biol Chem*, *293*(36), 13946-13960.
641 doi:10.1074/jbc.RA118.003916
- 642 Nicolas, A., Kenna, K. P., Renton, A. E., Ticozzi, N., Faghri, F., Chia, R., . . . Landers, J. E. (2018).
643 Genome-wide Analyses Identify KIF5A as a Novel ALS Gene. *Neuron*, *97*(6), 1268-
644 1283 e1266. doi:10.1016/j.neuron.2018.02.027
- 645 Parikh, J. R., Askenazi, M., Ficarro, S. B., Cashorali, T., Webber, J. T., Blank, N. C., . . . Marto, J. A.
646 (2009). multiplierz: an extensible API based desktop environment for proteomics
647 data analysis. *BMC Bioinformatics*, *10*, 364. doi:10.1186/1471-2105-10-364

- 648 Pease-Raissi, S. E., Pazyra-Murphy, M. F., Li, Y., Wachter, F., Fukuda, Y., Fenstermacher, S. J., .
649 . . Segal, R. A. (2017). Paclitaxel Reduces Axonal Bclw to Initiate IP3R1-Dependent
650 Axon Degeneration. *Neuron*, 96(2), 373-386 e376. doi:10.1016/j.neuron.2017.09.034
651 Pernigo, S., Chegkazi, M. S., Yip, Y. Y., Treacy, C., Glorani, G., Hansen, K., . . . Steiner, R. A. (2018).
652 Structural basis for isoform-specific kinesin-1 recognition of Y-acidic cargo adaptors.
653 *Elife*, 7. doi:10.7554/eLife.38362
654 Sasaki, Y., Vohra, B. P., Lund, F. E., & Milbrandt, J. (2009). Nicotinamide mononucleotide
655 adenylyl transferase-mediated axonal protection requires enzymatic activity but not
656 increased levels of neuronal nicotinamide adenine dinucleotide. *J Neurosci*, 29(17),
657 5525-5535. doi:10.1523/JNEUROSCI.5469-08.2009
658 Shlevkov, E., Basu, H., Bray, M. A., Sun, Z., Wei, W., Apaydin, K., . . . Schwarz, T. L. (2019). A
659 High-Content Screen Identifies TPP1 and Aurora B as Regulators of Axonal
660 Mitochondrial Transport. *Cell Rep*, 28(12), 3224-3237 e3225.
661 doi:10.1016/j.celrep.2019.08.035
662 Silva, J. C., Gorenstein, M. V., Li, G. Z., Vissers, J. P., & Geromanos, S. J. (2006). Absolute
663 quantification of proteins by LCMSE: a virtue of parallel MS acquisition. *Mol Cell
664 Proteomics*, 5(1), 144-156. doi:10.1074/mcp.M500230-MCP200
665 Sleight, J. N., Rossor, A. M., Fellows, A. D., Tosolini, A. P., & Schiavo, G. (2019). Axonal transport
666 and neurological disease. *Nat Rev Neurol*. doi:10.1038/s41582-019-0257-2
667 Thomas-Jinu, S., Gordon, P. M., Fielding, T., Taylor, R., Smith, B. N., Snowden, V., . . . Houart, C.
668 (2017). Non-nuclear Pool of Splicing Factor SFPQ Regulates Axonal Transcripts
669 Required for Normal Motor Development. *Neuron*, 94(2), 322-336 e325.
670 doi:10.1016/j.neuron.2017.03.026
671 Yamazaki, T., Souquere, S., Chujo, T., Kobelke, S., Chong, Y. S., Fox, A. H., . . . Hirose, T. (2018).
672 Functional Domains of NEAT1 Architectural lncRNA Induce Paraspeckle Assembly
673 through Phase Separation. *Mol Cell*, 70(6), 1038-1053 e1037.
674 doi:10.1016/j.molcel.2018.05.019
675 Zhu, H., Lee, H. Y., Tong, Y., Hong, B. S., Kim, K. P., Shen, Y., . . . Park, H. W. (2012). Crystal
676 structures of the tetratricopeptide repeat domains of kinesin light chains: insight into
677 cargo recognition mechanisms. *PLoS One*, 7(3), e33943.
678 doi:10.1371/journal.pone.0033943
679
680

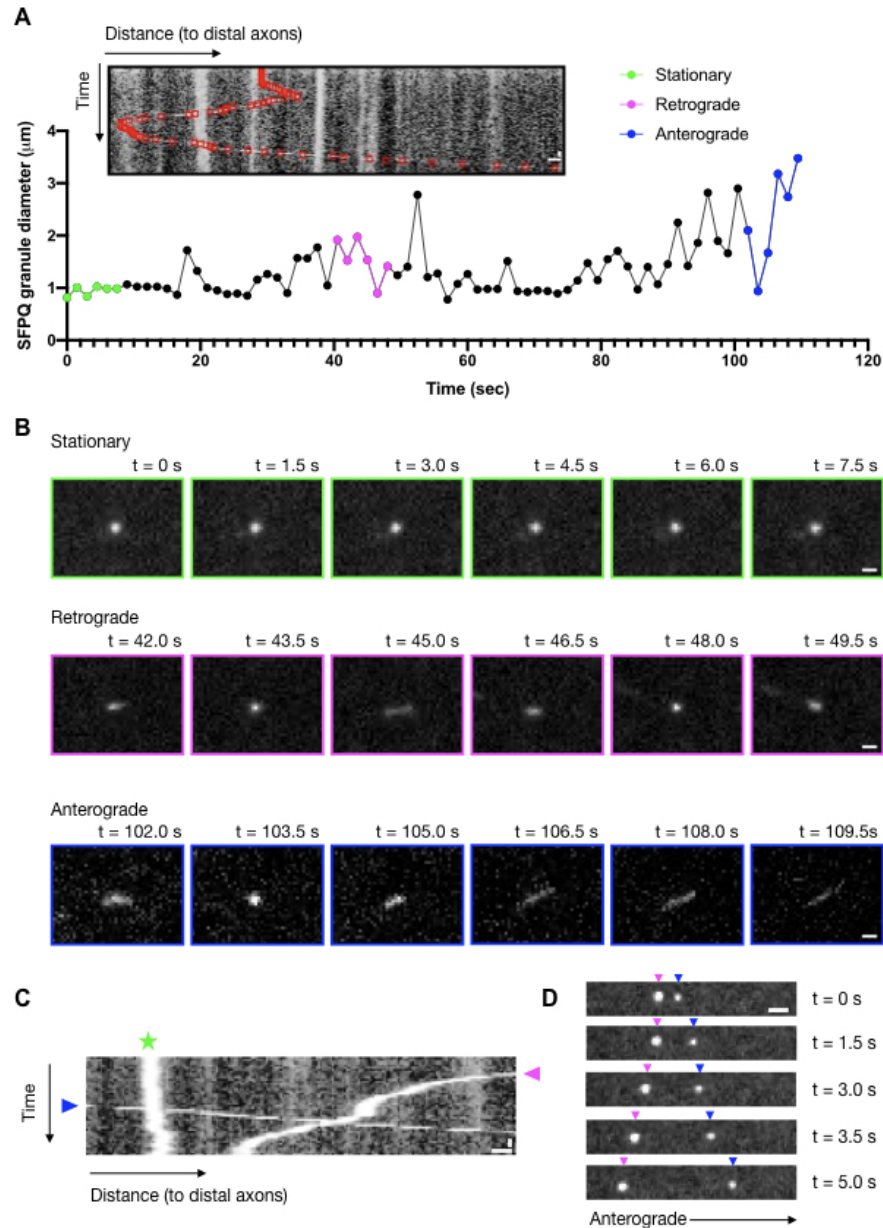
681 **Figures with Legends**



682
683
684
685
686
687

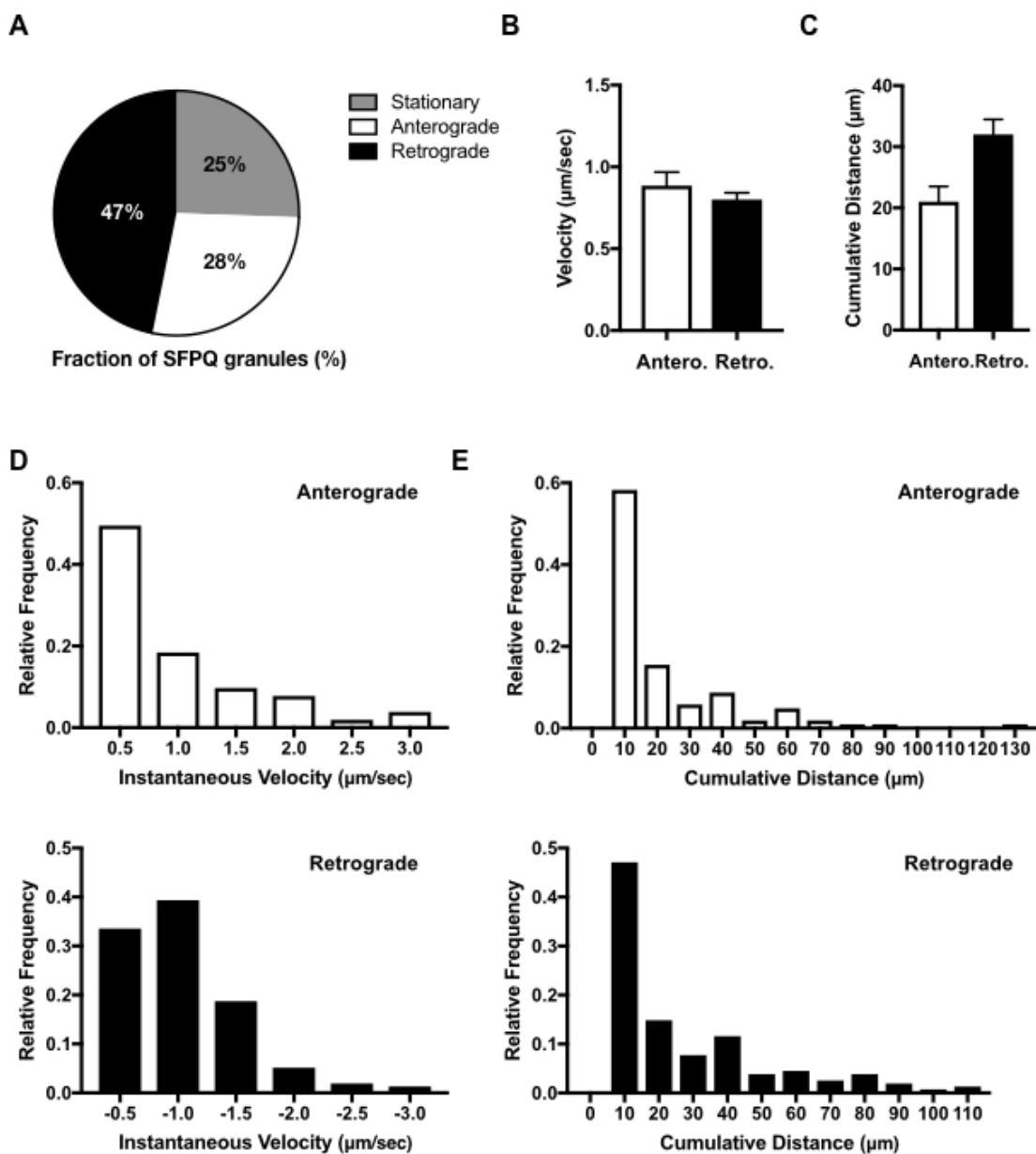
Introduction-figure supplement 1. Bioinformatic analysis of SFPQ protein sequence.

Schematic of protein domains of SFPQ and the probability score of SFPQ sequence for being disordered and prion-like as predicted by IUPred2 (top) and PLAAC (bottom), respectively.



688
689 **Figure 1. SFPQ granule, a non-membrane enclosed organelle, undergoes fast axonal transport.**
690 (A) Kymograph of a Halo-SFPQ granule transitioning through stationary, retrograde and anterograde
691 transport and its diameter plotted over time. Scale bars: 2 μm and 6 sec. (B) Time-lapse images of the
692 corresponding Halo-SFPQ granule from (A) in stationary (green), retrograde (magenta) and anterograde
693 (blue) phase. Scale bars: 1 μm . (C) Kymograph depicting representative Halo-SFPQ in stationary (green
694 star), anterograde (blue arrowhead) and retrograde (magenta arrowhead) phase. Scale bars: 2 μm and 6
695 sec. (D) Representative time-lapse images of Halo-SFPQ in axons of DRG sensory neurons moving in
696 anterograde (blue arrowhead) or retrograde (magenta arrowhead) direction. Scale bar: 2 μm .

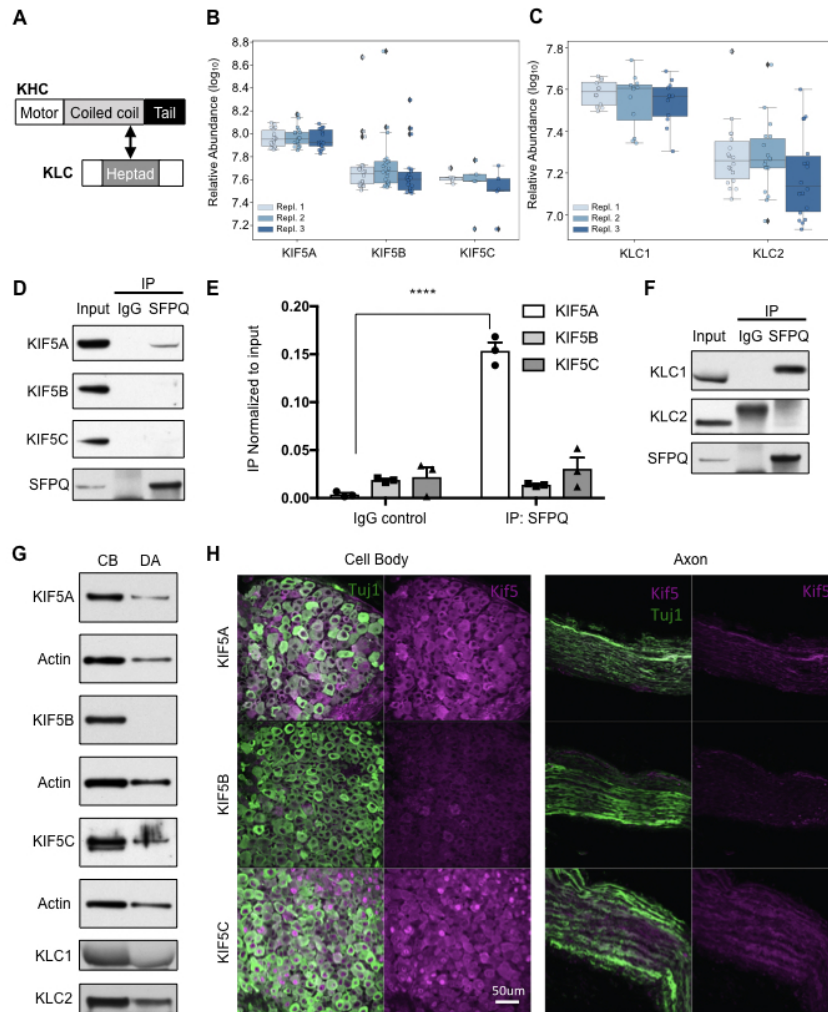
697
698 **Figure 1-figure supplement 1. Transport kinetics of SFPQ granules in axons of DRG sensory neurons.**



699
700
701
702
703
704
705
706

Figure 1-figure supplement 1. Transport kinetics of SFPQ granules in axons of DRG sensory neurons.

(A) Fraction of SFPQ granules spent in stationary, anterograde or retrograde phase. Data analyzed from 217 particles, from 29 axons, across 2 independent experiments. (B) Average velocity and (C) average cumulative distance of Halo-tagged SFPQ granules in axons and its frequency distribution in (D) and (E), respectively.



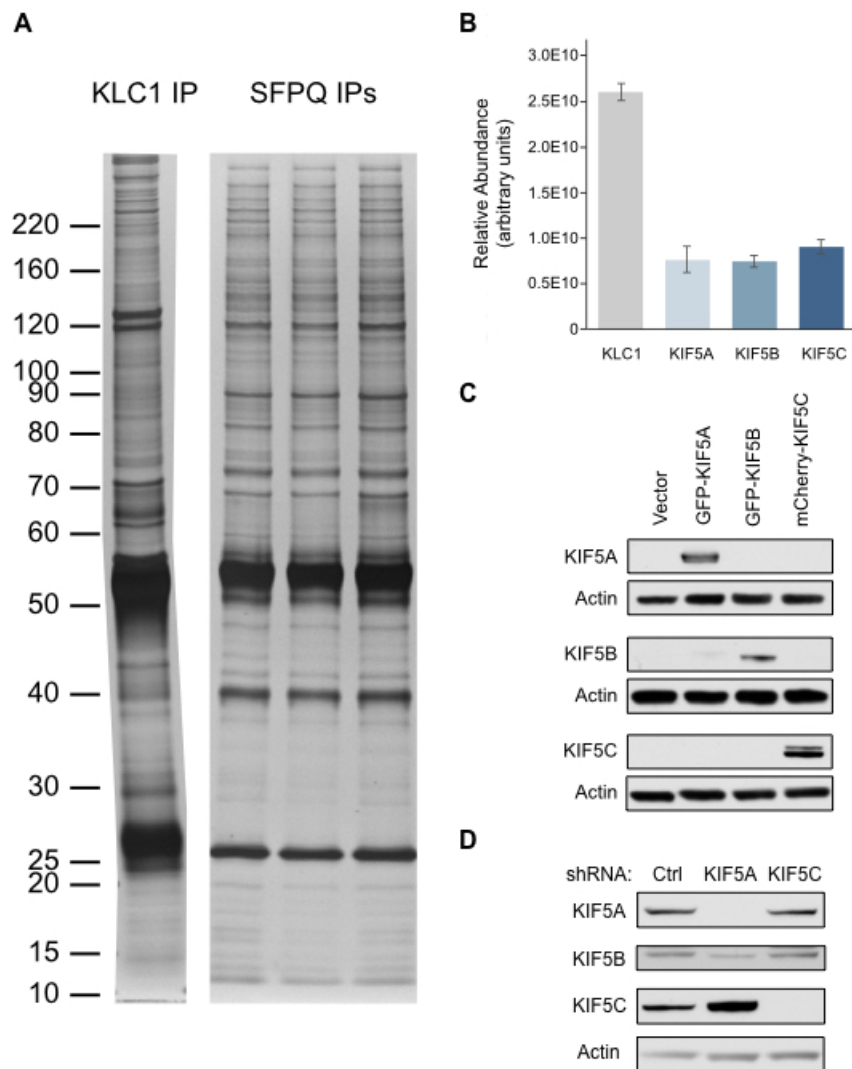
707
708
709
710
711
712
713
714
715
716
717
718
719
720
721
722
723
724
725
726

Figure 2. SFPQ preferentially binds to KIF5A/KLC1 motor complex.

(A) Schematic of domains of kinesin heavy chain (KHC) and kinesin light chain (KLC) and the interacting region between the heptad repeat of KLC and the coiled coil of KHC. (B and C) Box and whisker plot showing the relative abundance of KIF5A, KIF5B and KIF5C (B); and KLC1 and KLC2 (C) peptides derived from parallel reaction monitoring mass spectrometry. Data were acquired across three independent SFPQ immunoprecipitations (IPs). (D) IP of endogenous SFPQ from DRG sensory neuron protein lysate and blotted against endogenous KIF5A, KIF5B and KIF5C; IgG serves as control IP. (E) Quantification of pull down in (D) relative to input; ****p < 0.0001 by one way ANOVA; n = 3 independent IPs; data represent mean ± s.e.m. (F) IP of endogenous SFPQ from DRG sensory neuron protein lysate and blotted against endogenous KLC1 and KLC2; IgG serves as control IP. (G) Western blot of DRG neuron lysates of cell body (CB) and distal axons (DA) prepared from compartmented Campenot cultures probed against endogenous KIF5A, KIF5B, KIF5C, KLC1 and KLC2; actin serves as loading control. (H) Representative staining of endogenous KIF5A, KIF5B and KIF5C in DRGs and sciatic nerve of P1 mice; n = 4 independent staining of tissues; scale bar 50 µm; Tuj1 (Green), Kif5 (Magenta).

Figure 2-figure supplement 1. Silver stain analysis of endogenous KLC1 and SFPQ IPs from DRGs and verification of antibodies for KIF5A, KIF5B and KIF5C.

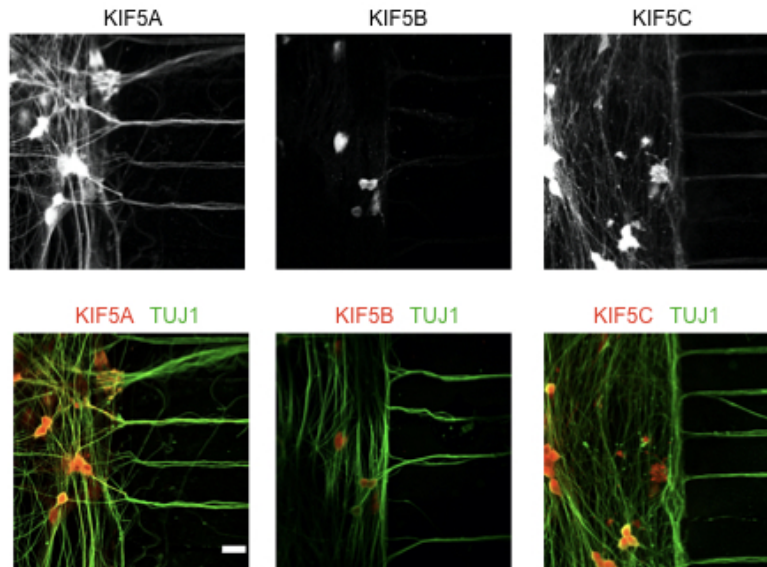
Figure 2-figure supplement 2. KIF5 motors differentially localizes to cell body and distal axons.



727
728 **Figure 2-figure supplement 1. Silver stain analysis of endogenous KLC1 and SFPQ IPs from DRGs and**
729 **verification of antibodies for KIF5A, KIF5B and KIF5C.**

730 (A) Silver stain analysis of endogenous KLC1 and SFPQ proteins purified from DRG extracts. Each lane
731 corresponds to 50% of the enriched material analyzed in Figure 2-figure supplement 1B (KLC1 IP) and
732 Figure 2B and 2C (three independent SFPQ IPs). (B) Relative abundance of KIF5A, KIF5B and KIF5C proteins
733 (with KLC1 as a reference) in a KLC1 IP measured by label-free mass spectrometry. Data represent mean
734 \pm s.e.m across two technical replicate analyses. (C) Western blot of HEK 293T lysates transfected with
735 empty vector, GFP-KIF5A, GFP-KIF5B or mCherry-KIF5C and probed with the KIF5 antibodies. Actin serves
736 as loading control. (D) DRG sensory neuron lysates infected with control (Ctrl) or with either shRNA against
737 *KIF5A* or *KIF5C* and probed with the KIF5 antibodies. Actin serves as loading control.

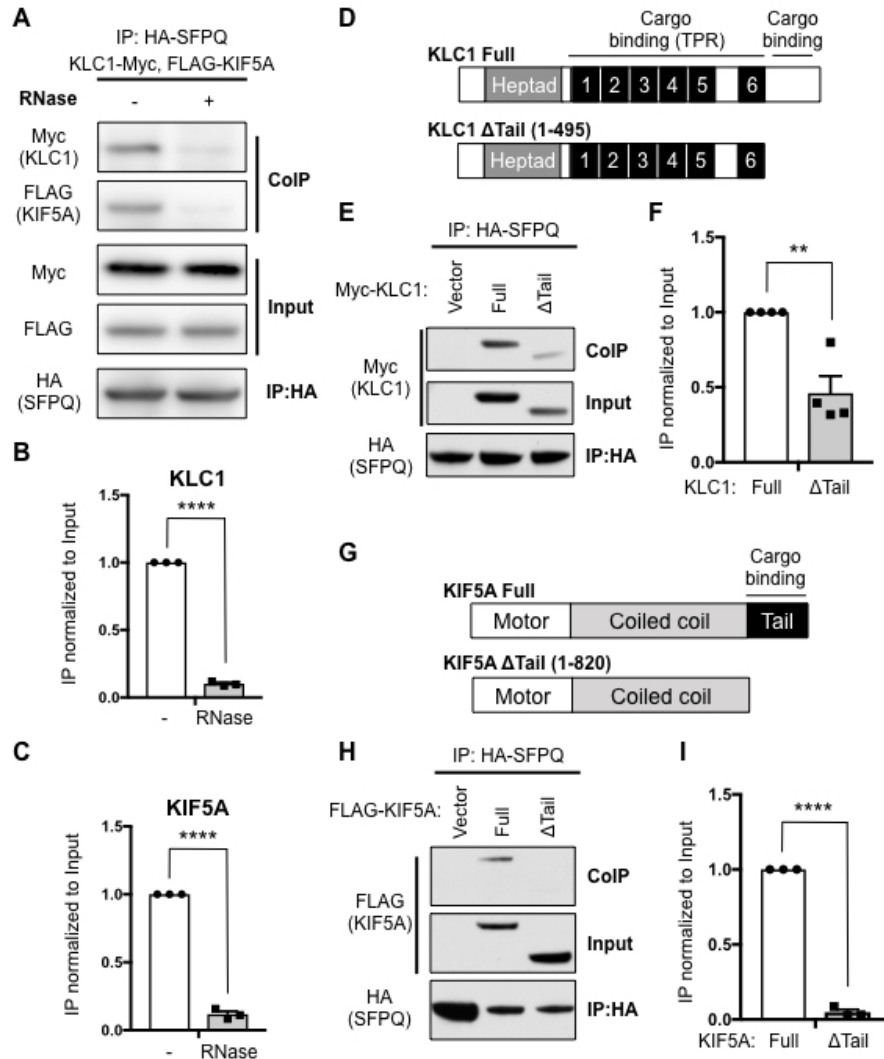
738



739
740
741
742

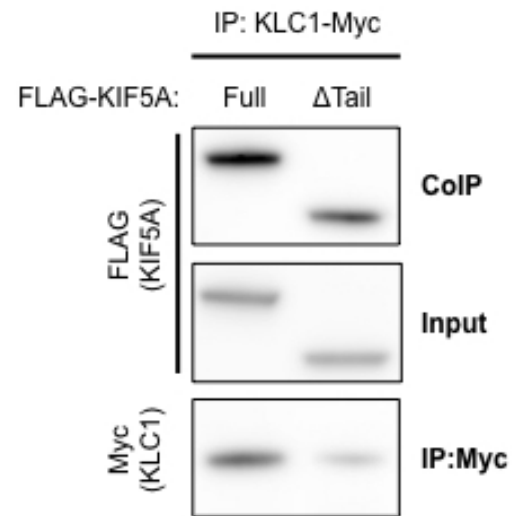
Figure 2-figure supplement 2. KIF5 motors differentially localize to cell body and distal axons.

Representative staining of endogenous KIF5A, KIF5B and KIF5C in DRG sensory neurons grown in microfluidic chambers; Scale bar 20 μ m; TUJ1 (green), KIF5 (Red).



743
 744 **Figure 3. RNase prevents SFPQ-RNA binding to KIF5A/KLC1.**
 745 (A) HEK 293T cells transfected with HA-SFPQ, FLAG-KIF5A and KLC1-Myc and lysates were treated with or
 746 without RNase. HA was IPed and blotted for HA, Myc and FLAG. (B) Quantification of pull down of KLC1-
 747 Myc in (A) relative to input; **** $p < 0.0001$ by unpaired two-tailed t test; $n = 3$; data represent mean \pm
 748 s.e.m. (C) Quantification of pull down of FLAG-KIF5A in (A) relative to input; **** $p < 0.0001$ by unpaired
 749 two-tailed t test; $n = 3$; data represent mean \pm s.e.m. (D) Schematic of the indicated constructs for KLC1;
 750 Heptad, Heptad repeat; TPR, tetratricopeptide repeat. (E) HEK 293T cells transfected with HA-SFPQ with
 751 empty vector, full length WT or tail-truncated Myc-KLC1. HA was IPed and blotted for Myc and HA. (F)
 752 Quantification of pull down in (E) relative to input; ** $p = 0.0033$ by unpaired two-tailed t test; $n = 4$; data
 753 represent mean \pm s.e.m. (G) Schematic of the indicated constructs for KIF5A. (H) HEK 293T cell transfected
 754 with HA-SFPQ with empty vector, full length WT or tail-truncated FLAG-tagged KIF5A. HA was IPed and
 755 blotted for FLAG and HA. (I) Quantification of pull down in (H) relative to input; **** $p < 0.0001$ by unpaired
 756 two-tailed t test; $n = 3$; data represent mean \pm s.e.m.

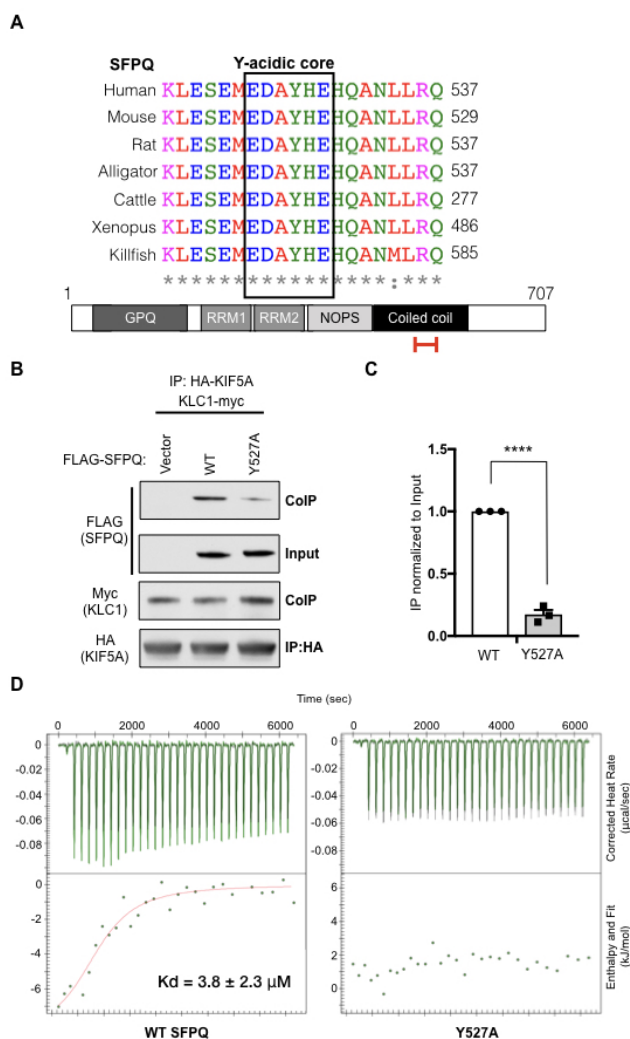
757
 758 **Figure 3-figure supplement 1. KIF5A Δ Tail mutant binds to KLC1.**
 759



760
761
762
763
764

Figure 3-figure supplement 1. KIF5A Δ Tail mutant binds to KLC1.

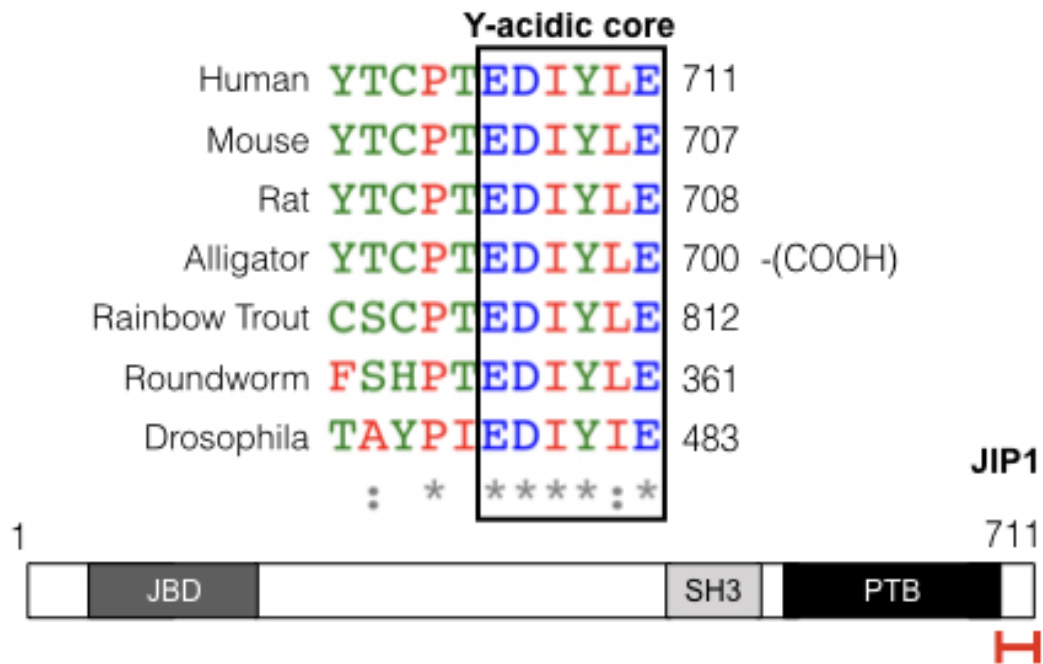
HEK 293T cells transfected with KLC1-Myc and with either WT FLAG-tagged KIF5A or the Δ Tail mutant. Myc was IPed and blotted for FLAG and Myc.



765
 766 **Figure 4. SFPQ directly binds to KLC1 through a Y-acidic motif within its coiled coil domain.**
 767 (A) Alignment of the sequence within the coiled coil domain of SFPQ containing the Y-acidic motif. On the
 768 bottom; schematic of the domains of SFPQ. Red bracket indicates the region containing the Y-acidic motif.
 769 GPO, glycine proline glutamine-rich; RRM, RNA recognition motif; NOPS, NONA/paraspeckle domain. (B)
 770 HEK 293T cells transfected with HA-KIF5A, KLC1-Myc and with either empty vector, full length WT or
 771 Y527A FLAG-tagged SFPQ. HA was IPed and blotted for FLAG, Myc and HA. (C) Quantification of pull down
 772 in (B) relative to input; ****p < 0.0001 by unpaired two-tailed t test; n = 3; data represent mean ± s.e.m.
 773 (D) Isothermal titration calorimetry (ITC) measurements of the reference KLC1 (TPR1-6) fragment with
 774 either the WT peptide (ESEMEDAYHEHQANLLR) or the Y-acidic mutant, Y527A, peptide
 775 (ESEMEDAHEHQANLLR) of SFPQ.

776
 777 **Figure 4-figure supplement 1.** SFPQ and JIP1 both share a Y-acidic motif.

778 **Table 1.** ITC parameters between KLC1 TPR1-6 fragment and WT SFPQ or Y527A Y-acidic mutant peptide.



779
780

781 **Figure 4-figure supplement 1. SFPQ and JIP1 both share a Y-acidic motif.**

782 Alignment of the sequence within the C-terminal region of JIP1 containing the Y-acidic motif. On the
783 bottom; schematic of the domains of JIP1. Red bracket indicates the region containing the Y-acidic motif.
784 JBD, JNK binding domain; SH3, Src homology-3 domain; PTB, phosphotyrosine binding domain.

785 **Table 1. ITC parameters between KLC1 TPR1-6 fragment and WT SFPQ or Y527A Y-acidic mutant**
786 **peptide.**

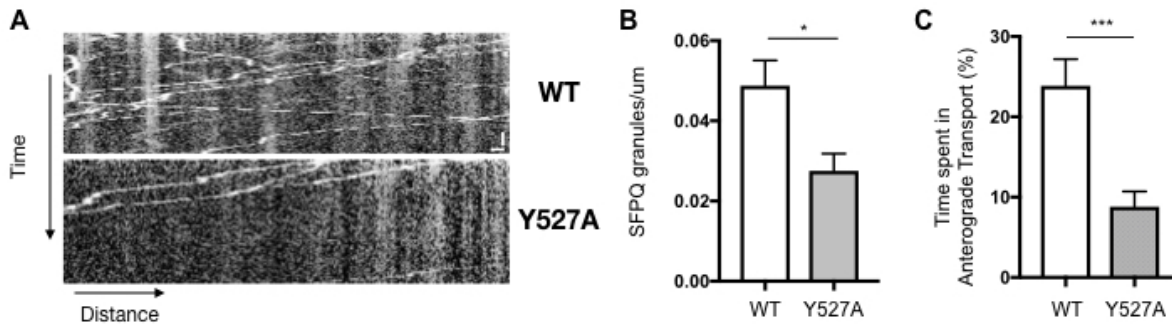
787

KLC1 TPR1-6 (Cell)	SFPQ (Syringe)	N	Kd (μM)	ΔH (kJ/mol)	ΔS (J/mol·K)
	WT	0.964 \pm 0.143	3.833 \pm 2.310	-8.580 \pm 1.834	74.92
	Y527A	No Binding			

788

789 **Table1-Source Data 1:** Raw ITC data for WT SFPQ

790 **Table1-Source Data 2:** Raw ITC data for Y527A Y-acidic mutant



791

792

Figure 5. Direct binding of SFPQ to KIF5A/KLC1 is required for its transport in axons.

793

(A) Representative kymograph of WT and Y527A Halo-tagged SFPQ. Scale Bars: 2 μm and 15 sec. (B)

794

Average number of Halo-tagged WT and Y527A per micron of axon length. Analyzed from n = 25-33 axons

795

from two independent experiments; *p = 0.0117; data represent mean \pm s.e.m. (C) Average percentage

796

of time spent in anterograde transport for Halo-tagged WT and Y527A in axons of DRG sensory neurons.

797

Analyzed from n = 25-33 axons from 2 independent experiments; ***p = 0.0005; data represent mean \pm

798

s.e.m.

799

800

Figure 5-figure supplement 1. SFPQ mode of binding to KLC1 is distinct from JIP1.



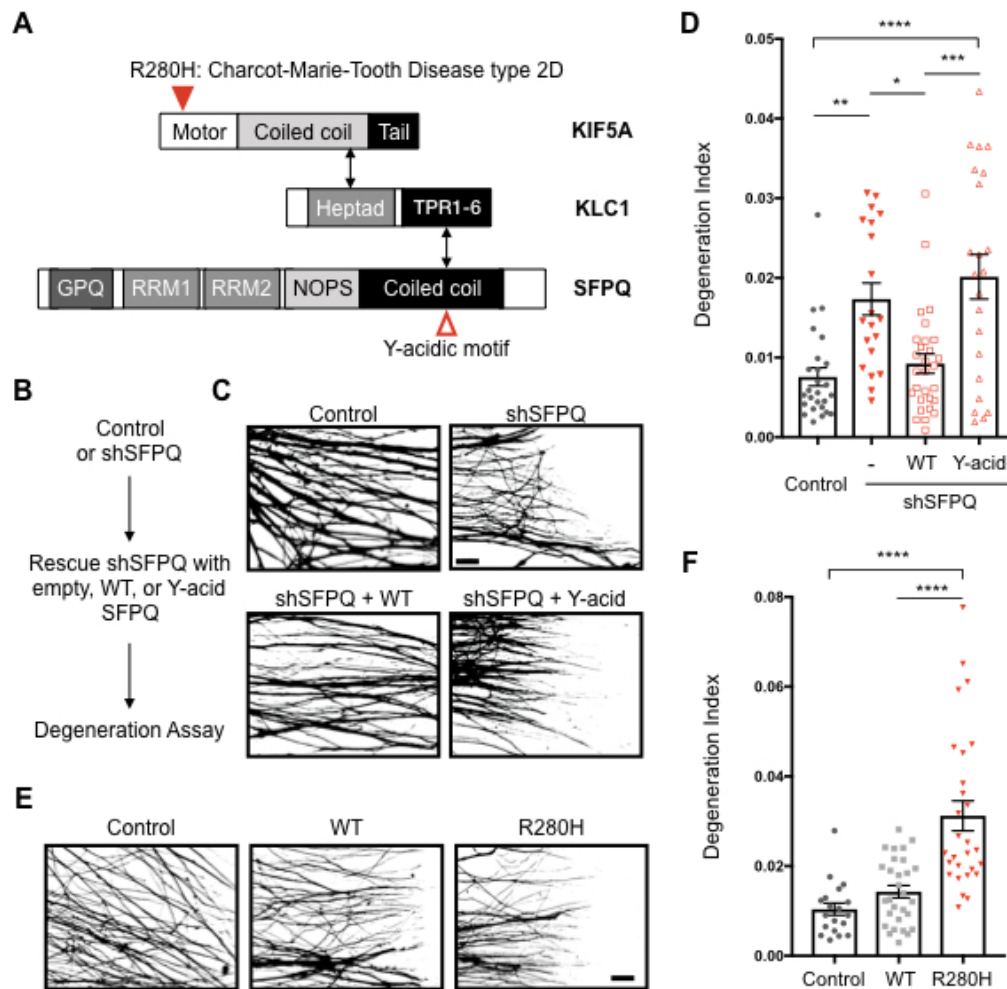
801

802 **Figure 5-figure supplement 1. SFPQ mode of binding to KLC1 is distinct from JIP1.**

803 (A) Schematic cartoon depicting the location of N343 on KLC1 in comparison to KLC2 on A helix of TPR4.

804 (B) HEK 293T lysates transfected with HA-SFPQ, and with either Myc-tagged WT or N343S mutant of KLC1.

805 HA-SFPQ was IPed and blotted against HA and Myc.



806
807 **Figure 6. Defect in KIF5A-driven transport of SFPQ leads to axon degeneration in DRG sensory**
808 **neurons.**

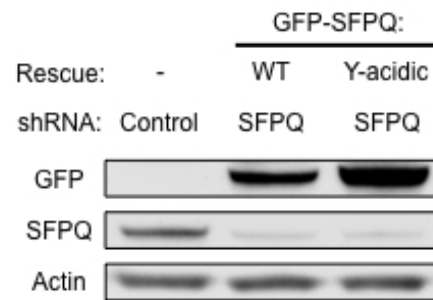
809 (A) A schematic representation of KIF5A, KLC1 and SFPQ. Red closed arrowhead indicates the location of
810 R280H CMT2D mutation; and open arrowhead indicates the location of Y-acidic motif of SFPQ. (B) A
811 flowchart of rescue experiment of degeneration assay using WT or the Y-acidic mutant of SFPQ. (C)
812 Representative binarized Tuj1-labeled axons in compartmented cultures expressing control (n = 26) or
813 shSFPQ rescued with empty vector (n = 20), WT (n = 29) or the Y-acidic mutant (n = 22) of SFPQ. From 3
814 independent experiments; Scale bar 100 μ m. (D) Quantification of axon degeneration index of (C); *p =
815 0.0112, **p = 0.0019, ***p = 0.0002, ****p < 0.0001 by one way ANOVA; data represent mean \pm s.e.m.
816 (E) Representative binarized Tuj1-labeled axons in compartmented cultures expressing control (n = 19),
817 WT (n = 29) or R280H (n = 28) mutant of KIF5A. From 3 independent experiments; Scale bar 100 μ m. (F)
818 Quantification of axon degeneration index of (E); ****p < 0.0001 by one way ANOVA; data represent
819 mean \pm s.e.m.

820

821 **Figure 6-figure supplement 1.** Expression of shRNA-resistant WT or Y-acidic GFP-tagged SFPQ.

822 **Figure 6-figure supplement 2.** R280H mutation of KIF5A, which impairs transport, also reduces binding
823 to SFPQ.

824



825

826

827

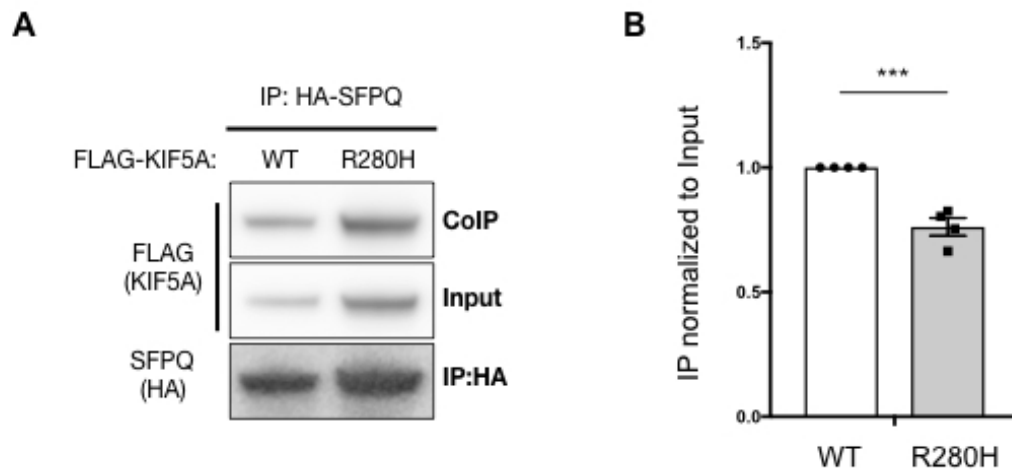
828

829

830

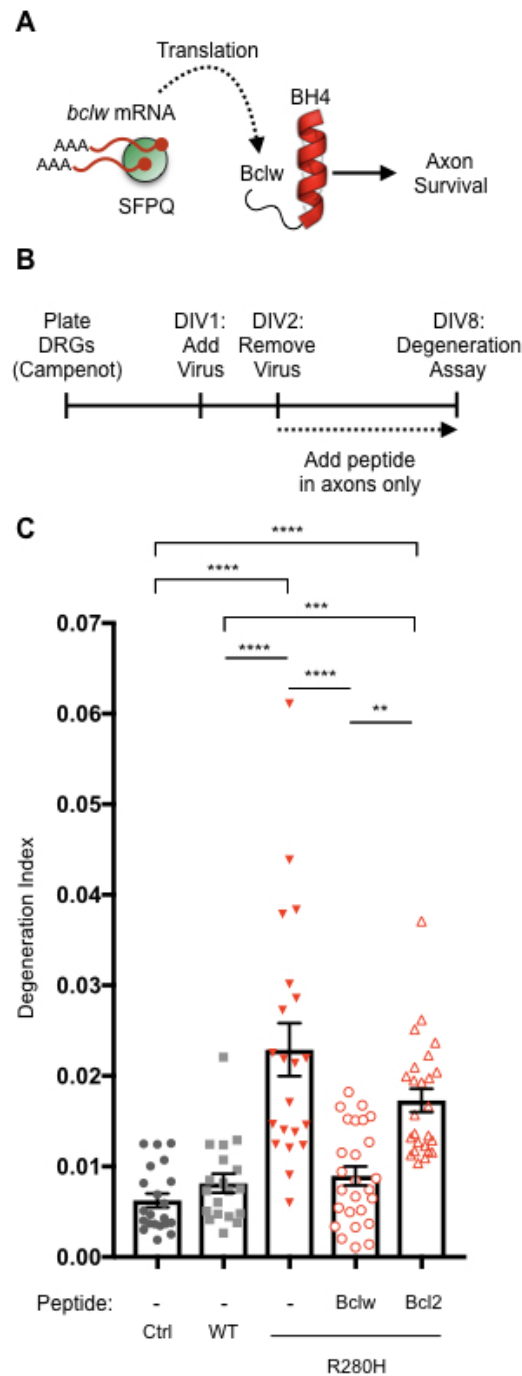
Figure 6-figure supplement 1. Expression of shRNA-resistant WT or Y-acidic GFP-tagged SFPQ.

DRG neurons were infected with control or shRNA against SFPQ and rescued with empty, GFP-tagged WT or Y-acidic mutant of SFPQ. Protein lysates were blotted against GFP, endogenous SFPQ and actin as loading control.



831
832 **Figure 6-figure supplement 2. R280H mutation of KIF5A, which impairs transport, also reduces binding**
833 **to SFPQ.**

834 (A) HEK 293T lysates transfected with HA-SFPQ, and with either FLAG-tagged WT or R280H mutant of
835 KIF5A. HA-SFPQ was IPed and blotted against FLAG and HA. (B) Quantification of pull down in (A)
836 normalized to input. *** $p = 0.0006$ by unpaired two-tailed t test; $n = 4$; data represent mean \pm s.e.m.



837
 838 **Figure 7. Axon degeneration caused by CMT2D R280H KIF5A mutation can be rescued by a Bclw**
 839 **mimetic peptide.**

840 (A) A schematic of pathway for axon survival mediated by SFPQ. (B) Flowchart of Bclw peptide rescue
 841 experiment in DRG neurons cultured in compartmented Campanot chambers. (C) Quantification of axon
 842 degeneration index of control (Ctrl; n = 21), WT KIF5A (n = 19), R280H with either no peptide (n = 21), Bclw
 843 (n = 26), or Bcl2 peptide (n = 25). From 3 independent experiments; **p = 0.0011, ***p = 0.0010, ****p
 844 < 0.0001 by one way ANOVA; data represent mean \pm s.e.m.
 845

846 **Introduction-figure supplement 1.** Bioinformatic analysis of SFPQ protein sequence.
847 **Figure 1-figure supplement 1.** Transport kinetics of SFPQ granules in axons of DRG sensory neurons.
848 **Figure 2-figure supplement 1.** Silver stain analysis of endogenous KLC1 and SFPQ IPs from DRGs and
849 verification of antibodies for KIF5A, KIF5B and KIF5C.
850 **Figure 2-figure supplement 2.** KIF5 motors differentially localizes to cell body and distal axons.
851 **Figure 3-figure supplement 1.** KIF5A Δ Tail mutant binds to KLC1.
852 **Figure 4-figure supplement 1.** SFPQ and JIP1 both share a Y-acidic motif.
853 **Figure 5-figure supplement 1.** SFPQ mode of binding to KLC1 is distinct from JIP1.
854 **Figure 6-figure supplement 1.** Expression of shRNA-resistant WT or Y-acidic GFP-tagged SFPQ.
855 **Figure 6-figure supplement 2.** R280H mutation of KIF5A, which impairs transport, also reduces binding
856 to SFPQ.
857
858 **Table 1.** ITC parameters between KLC1 TPR1-6 fragment and WT SFPQ or Y527A Y-acidic mutant
859 peptide.
860 **Table1-Source Data 1:** Raw ITC data for WT SFPQ
861 **Table1-Source Data 2:** Raw ITC data for Y527A Y-acidic mutant
862
863 **Supplementary File 1:** LC-MS/MS data
864
865 **Video 1:** Halo-SFPQ is transported in anterograde and retrograde manner in axons. Time-lapse movie
866 was captured in axons of dorsal root ganglion sensory neurons grown in compartmented cultures. The
867 video was acquired every 1.5 sec and played at 10 fps.
868 **Video 2:** Y527A mutation of SFPQ disrupts axonal transport of SFPQ. Time-lapse movie was captured in
869 axons of dorsal root ganglion sensory neurons grown in compartmented cultures. The video was
870 acquired every 1.5 sec and played at 10 fps.